8-4-2020

Development of a Nomogram to Predict the Maximum Contact Stress Between a Bridge I-Girder and a Support Roller

Thanin Chanmalai

THE UNIVERSITY OF NEW HAVEN

DEVELOPMENT OF A NOMOGRAM TO PREDICT THE MAXIMUM CONTACT STRESS BETWEEN A BRIDGE I-GIRDER AND A SUPPORT ROLLER

A THESIS

Submitted in partial fulfillment

of the requirements for the degree of

MASTER OF SCIENCE IN CIVIL ENGINEERING

BY

Thanin Chanmalai

University of New Haven
West Haven, Connecticut
August 4th, 2020

DEVELOPMENT OF A NOMOGRAM TO PREDICT THE MAXIMUM CONTACT STRESS BETWEEN A BRIDGE I-GIRDER AND A SUPPORT ROLLER

APPROVED BY

Byungik Chang, Ph.D., P.E., M.B.A.
Thesis Advisor

Samuel Bogan Daniels, Ph.D., P.E.
Committee Member

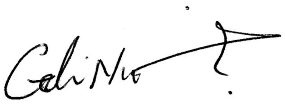

Goli Nossoni, Ph.D.
Program Coordinator and Committee Member

Ronald Surendran Harichandran, Ph.D., P.E.
Dean of the College

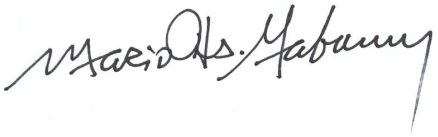

Mario Thomas Gaboury, J.D., Ph.D.
Interim Provost & Senior Vice President for Academic Affairs

ACKNOWLEDGEMENTS

The successful completion of this research report and the study discussed herein would not have been achievable without the recommendation and assistance of my graduate advisor, Dr. Byungik Chang. The knowledge and estimable work ethic he imparted to me will continue to serve in all my future endeavors. I also would like to thank the staff and faculty in the Department of Civil and Environmental Engineering at the University of New Haven, who has provided the most cooperative assistance to this research work. I would like to thank Drs. Samuel Bogan Daniels and Goli Nossoni for serving on the thesis committee. I would like to thank my parents, Thavee and Wipawadee, for supporting me and inspiration in my life as I pursued my education at the University of New Haven. The authors would like to acknowledge the Royal Thai Army for the support of the research. I also would like to thank one of my best friends, Mr. Christopher Ong, who provide many materials and great support for my research work at the University of New Haven.

ABSTRACT

The incremental launching method (ILM) is one of the methods of bridge construction located in environmentally sensitive areas. During the bridge launching, there are significant contact stress issues at the contact regions between the launching system and the steel bridge girders. The Iowa River Bridge (IRB) is a case study of bridge construction that used the ILM during a steel I-girders installation. Contact stress can cause severe defects during launch, which can occur within the material where the material could be damaged.

Hertz contact theory is applied for calculating contact stress between two solid surfaces, which is initially derived from the contact between cylinder and plane surface. However, Hertz contact theory can calculate only the contact area and stress between two elastic solids with specific modeling in equilibrium. The solutions of the launching girder bridge construction's contact stress are not usually possible with closed-form Hertz contact theory solutions because of the complex geometries, loads, and material properties.

Typically, the issues, including complicated structural systems, need to rely on numerical modeling such as the finite element analysis (FEA) from ANSYS®. The primary objective of this study is to provide an estimate the relationship of the maximum contact stress between an I-girder and a roller using a nomogram. The nomogram is built based on a parametric study with various roller dimensions and vertical loads by numerical modeling. A total of 180 numerical models were used to develop the contract stress nomogram. The maximum contact stress from the nomogram can be useful tool in designing a bridge girder on a support roller.

TABLE OF CONTENTS

LIST OF TABLES

LIST OF FIGURES

CHAPTER 1. INTRODUCTION

1.1 Problem statement

The incremental launching method (ILM) has achieved to consider for bridge construction in recent years as one of the bridge erection methods. In this method, the bridge superstructure is constructed on one side of the pier to be crossed and then launched into its final state)LaViolette , 2007(. The launching is typically delivered in a range of increments so that additional sections can be added to the rear of the superstructure unit before succeeding launches. As one example, the Iowa River Bridge (IRB) on Highway 20 in north-central Iowa crossing an environmentally sensitive river belt, was constructed by the ILM to minimize the environmental impacts)Wipf, et al., 2004(as illustrated in Figure 1.1 (a). During the bridge launching, there are significant forces that can be generated between the launching system and steel I-girder as shown in Figure 1.1 (b). As expected, high contact stresses would be created in the small contact area where the roller and the lower surface of the bottom flange of a steel I-girder are in contact. The described small contact area with applied forces could cause severe damage to the structure. The Hertz contact theory is not applicable to the contact condition between the roller and the bottom flange of I-girder due to the complex geometry and loads. Typically, the complicated structural systems need to rely on numerical modeling such as the finite element analysis (FEA) to obtain detailed information.

(a) Aerial view of launching worksite and girder bracing)LaViolette , 2007(

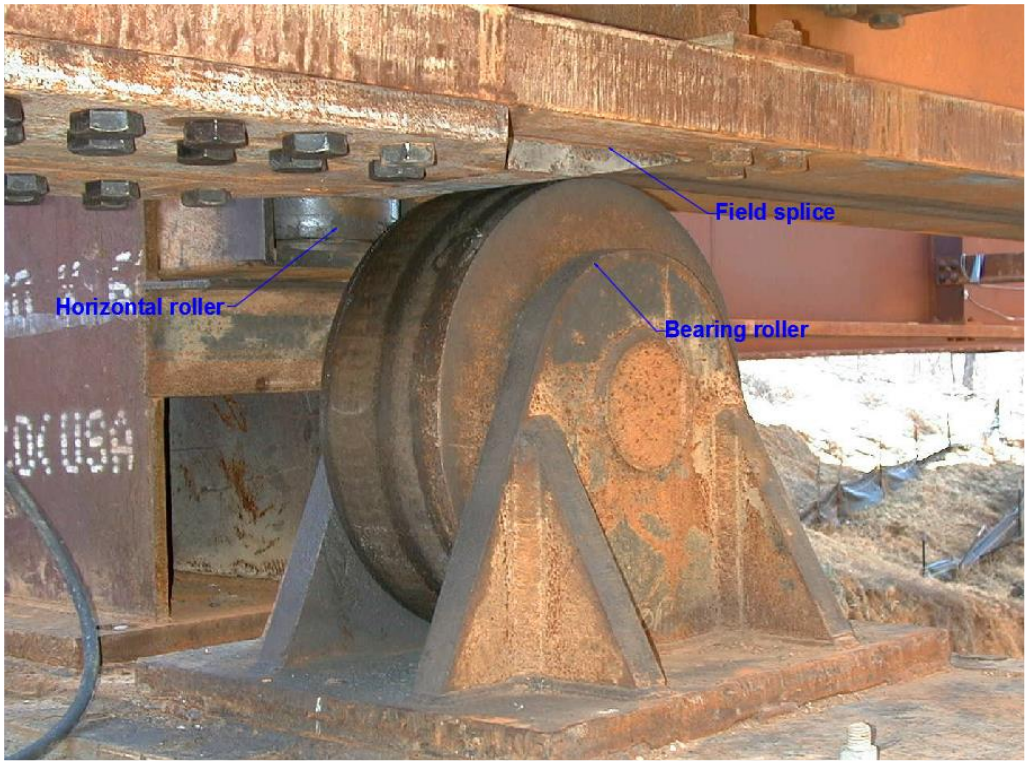

(b) Roller support and guide roller during launching)Wipf, et al., 2004(

Figure 1.1 General view of Iowa River Bridge launching

1.2 Objectives

The primary objective of this study is to estimate the relationship of the maximum contact stress between a bridge I-girder and a support roller. The proposed nomogram is built based on a parametric study by numerical modeling with various roller dimensions and loads. The maximum contact stress from the nomogram can be estimated quickly with ease. The nomogram could be a useful tool for predicting the maximum contact stress between a bridge girder and a support system. This study includes a preliminary modeling of the cylindrical contact to verify the Hertz contact theory)Hertz, 1896(. In addition, the field data that were collected during the IRB construction were used to ensure that the numerical modeling in the study can predict structural behavior. Since there are many factors to be considered in the modeling, a simplified numerical modeling was developed and compared with the initial numerical modeling. Lastly, a parametric study was performed with various roller diameter, roller width, and vertical loads to develop the contact stress nomogram.

1.3 Thesis outline

This thesis is formed by seven chapters. Chapter 1 presents general information about the purposes of the research. Chapter 2 illustrates the literature review, especially for the contact stress problems while Chapters 3 and 4 describe the overall background regarding the Hertz contact theory and validations modeling of the IRB. Chapter 5 introduces the simplified contact modeling that was developed and compared with the initial numerical modeling. Chapter 6 summarizes the numerical results from a parametric study with 180 contact models to develop the proposed nomogram to estimate the maximum contact stress between a bridge I-girder and a support roller. Chapter 7 provides the summary and conclusions of this study.

CHAPTER 2. LITERATURE REVIEW

Literature review is conducted to collect usable information about contact stress theory. Many relevant studies are reviewed and summarized. This chapter presents literature review with five sections: general contact stress theory, contact stress during bridge launching, behavior of an incrementally launched bridge, finite element analysis for contact problems, and mesh generation in finite element analysis.

2.1 Contact stress during bridge launching

In recent years, bridge construction over deep valleys, water crossings with steep slopes, or environmentally protected regions presents challenges that are be addressed by the incremental launching method (ILM). This method is one of bridge erections for such circumstance and the ILM offers advantages over conventional construction, which include creating a minimal disturbance to surroundings, providing a more concentrated work area for superstructure assembly, and possibly increased worker safety. A bridge superstructure in the ILM is constructed on one side of the pier to be crossed and then launched into its final state. The launching is typically delivered in a range of increments so that additional sections can be added to the rear of the superstructure unit before succeeding launches. During bridge launching, there are significant forces that can be generated between a bridge I-girder and a support roller. As expected, high contact stresses would be created in the small area where the roller and the lower surface of I-girder are in contact. The described small contact area with the reactions on the roller can cause severe damage to the structure. The Iowa River Bridge (IRB) was used as a case study of critical stresses between the bridge I-girder and the support roller due to concentrated forces at the contact region)Wipf, et al., 2004(. Moreover, the

contact stress on the lower surface of the launched girder is the vertical load, and a traveling load exists during the launch bridge)LaViolette , 2007(.

2.2 Contact stress theory

Hertz contact theory is based on the assumption that the contacting surfaces between the two geometries are frictionless, stress and strain of homogeneous material occur in the elastic limit, and the load is applied perpendicular to the surface)Hertz, 1896(. The contact stress based on Hertz contact theory between a cylinder and a plane surface can be determined using a nomogram that has been demonstrated by Norden. This literature identifies the Hertz contact theory equation regarding the contact stress and obtains the deformation that can be developed to determine the maximum contact stress)Norden, 1973(. In addition, Adams and Nosonovsky illustrated that Hertz presented the contact stress at the point of contact with a frictionless contact. Contact stresses and deformations satisfy the differential equations for stress and strain for homogeneous, isotropic, and elastic bodies in equilibrium. The stress passes at a considerable distance to the contact zone. The force is perpendicular to the surface and neglects the effect of surface shear stresses. Tangential stress components are zero between the contact zones. The stress integrated over the contact area equals the force pushing between two geometries. The two bodies touch each other within the contact zone, but the dimension of the contact zone is small compared to the radii of curvature of the bodies under load)Adams & Nosonovsky, 2000(.

Another study by Fischer and Wiest (2008) shows the numerical modeling based on Hertz contact theory to determine the contact stress between a wheel and a rail. To determine the wheel and rail contact problem, the proposed relationships are specific for a tiny spherical contact ellipse as they occur in the contact between a wheel and the middle section of a

crossing. The contact stress between a wheel and a rail from Hertz contact theory allows a direct application for the design purposes)Fischer & Wiest, 2008(.

The replacement of the elliptical integral with the polynomial system to be a consideration of the Hertz contact theory)Antoine & Abba, 2006(. In the roller bearing analysis, the mathematical calculations were achieved by using approximations of elliptical functions and with a numerical study of Hertz contact theory results. The polynomial approximations are used to determine the elliptic integrals to obtain an approximate analytical model of Hertz contact theory. This function can also be useful in optimization processes, especially in bearing design or in static and dynamic problems with bearings. Tanaka provides iterative methods for the solution of the contact region, the maximum contact stress, the interactive approach, and the contact spring constant, which yielded simple analytical expressions by examining the proportion of the elliptic semi-axis)Tanaka, 2001(.

However, Hertz contact theory is not applicable to the solutions of contact stress problems with closed-form solutions of contact stress between the bridge I-girder and the support roller because of the complicated geometries, loadings, and material properties.

2.3 Behavior of a bridge I-girder on a support roller

The response of the steel I-girders subjected to concentrated load can be investigated using finite element analysis (FEA) and comparisons with experimental data from the field. The research investigation for steel I-girder, influence with a load capacity that influences the material failure.

Chang (2004) studied the behavior of Iowa River Bridge with a focus on the contact stress between the steel I-girder and the support roller during launching using the numerical modeling. Chang considered the member-end force-based approach, girder aspect ratio to

minimize the modeling size, hexahedral mesh, material nonlinearity in his study)Chang, 2004(. However, Chang made an initial bonded condition between the girder and the roller in his modeling and this did not reflect the real contact condition.

Moreover, an experiment in a reducing scale test of the steel I-girder bridge was conducted by Chacon et al. (2013) and the results including strains, stresses, and displacements during launching were validated by the numerical modeling. The response of girders with slender webs subject to a concentrated load using nonlinear finite element analysis was compared with laboratory results)Chacon, Uribe, & Oller, 2013(.

The behavior of girder webs subjected to a local load with a concentrated load perpendicular to the flange on a plate girder was studied by Granath (1997) during the launching of the bridge. The failure behavior can be determined by the slenderness of the steel girder and the load condition. The investigated girder dimensions and the moment capacity of the flange did not influence the bearing capacity from the local load. The bending stiffness of the flange is used to determine the resistance)Granath, 1997(. The distribution of support reactions against a steel girder on a launching shoe was analyzed and compared among laboratory experiments, finite element analysis, and mathematical calculation. These three features are involved with the design of the reaction force when the steel girder was launched on a launching shoe with a slide bearing. The design calculations for the appropriate load were performed with equations valid for the case of a uniform distribution. The studies show that the support reaction has a non-uniform distribution of contact stress)Granath, 1998(.

2.4 Finite element analysis for contact problems

The contact stress analysis in a complicated structural system needs to rely on numerical modeling. Many researches have been performed using a numerical modeling approach to solve the contact problem.

Xin Zhao and Zili Li (2014) presented a transient finite element modeling approach to solve the frictional rolling contact problem. The research focused on the distributions of surface shear stress and micro-slip in the contact patch to investigate the relationships between material properties, plastic deformation, frictional contact, wear, and crack initiation (Zhao & Li, 2014). Wriggers (1996) approached the numerical modeling with friction when general constitutive equations are formulated in the contact interface. Applying a geometrical model and discretization for contact was validated for large deformations. Furthermore, the algorithms to integrate the interface laws were discussed for the tangential stress components)Wriggers, 1996(.

Xie and Adams (1995) presented an existing three-dimensional elastic plastic of the FEA by several point load. The modeled design was determined to create load and support cylinders in contact with a composite part efficiently. The accurately of the modeling compared related to a possible closed-form solutions and other rigorous contact modeling designs)Xie & Adams, 1995(. The examination of stresses and deformations occurring between two contact surfaces was performed by Mijovic and Dzoklo (2000). The finite element method was applied as a numerical procedure to obtain compressive stresses between two elastic geometries. The impact of the load effect on two geometries causes deformation along each contact surface that are usually nonlinear states. The contact region that is in touch between two components depends on loads, material property, and boundary conditions)Mijovi & Oklo, 2000(.

A contact mechanics modeling and simulation of the wheel-rail contact is introduced by Srivastava et al. (2014). The rail wheel contact analysis resulted in variable contact profiles which were applied to estimate the impact of contact stress distribution around the contact area. In this study, the finite element analysis was conducted to calculate fatigue failure parameters and the solutions for contact analysis of complicated geometries, as in the case of wheels and rail interaction. The stress decreased when increasing the wheel and rail profile radii. Additionally, the basis for the development of the wheels and rails configuration, fatigue resistance purpose, and examination outlining of the railroad can be identified by using the numerical modeling (Srivastava, Sarkar, & Ranjan, 2014). Gupta et al. (2012) applied the finite element analysis model of a spur gear assembly to compare the contact stress between two gears with the Hertz contact theory equation. Based on the result of the contact stress analysis, parametric models were created during the design of gear. The maximum contact stress decreases with increasing the geometric size)Gupta, Choubey, & Varde, 2012(.

2.5 Mesh generation in finite element analysis

Mesh generation for FEA is the discretization of the physical domain. Meshing is an essential step for the process to take place for numerical modeling with complex geometries that are divided into simple elements. The mesh affects the accuracy and speed of the simulation because meshing typically uses an essential portion of the time to generate reliable result. The computed solution will be reliable in the model, and the results as these elements are made finer by mesh refinement. After computing the numerical solution on the coarse mesh, the process of mesh refinement begins to improve the results. Typically, mesh refinement is the method of resolving the model with successively finer meshes by comparing

the different meshes' results. This comparison can be verified by comparing the field measurement at one or more points in the model.

Shiao and Chamis introduced the mapping method to improve the accuracy and efficiency of results. A hexahedral mesh can be generated to the complex geometries of the finite element analysis. According to the study, analyzing the entire geometry with coarse mesh was recommended. Then, creating finer meshed around only a specific region follows to get an accurate result with the reliable number of nodes equal to 361 (19 by 19))Shiao & Chamis, 1992(. In addition, mesh density between contact areas is found to influence the reliable results of the numerical modeling directly)Sladkowski & Sitarz, 2003(. To standardize the contact area analysis, mesh with an element size of 1 mm for all the configurations was chosen)Srivastava, Sarkar, & Ranjan, 2014(.

An appropriate mesh density is also significant to predict the stress performance of modeling. The refinement of mesh density in the concentration region improves a reliable result for FEA. The use of hexahedron elements can reduce the time needed to generate the mesh, which has the advantages in terms of reducing the number of elements and reliability improvement)Shepherd & Johnson, 2006(.

CHAPTER 3. HERTZ CONTACT THEORY VALIDATION

3.1 Hertz contact theory

This chapter discusses the preliminary modeling of the cylindrical contact to verify the Hertz contact theory to determine the maximum stress that occurred in the contact area. The load parameter and the cylinder section property are significant factors to the contact stress. ANSYS® was used for the numerical modeling.

The Hertz contact theory is based on the following assumptions: the contacting surfaces between the two geometries are frictionless, stress and strain of homogeneous material occur in the elastic limit, and the load is applied perpendicular to the surface)Antoine & Abba, 2006(.

The data assumed for Hertz contact theory validation for the study are following: force (F) of 2,500 lb_f, contact length (l) of 3 inches, cylinder diameter (d_1) of 18 inches, the diameter for plane surface define as infinite (See Figure 3.1), Elastic Modulus of 29,000 ksi for the steel d r d d r of 0.3 for both objects)Thorwald & Vargas, 2017(. Table 3.1 summaries the data used for the cylindrical contact of Hertz contact theory to compare with the numerical contact modeling in ANSYS®.

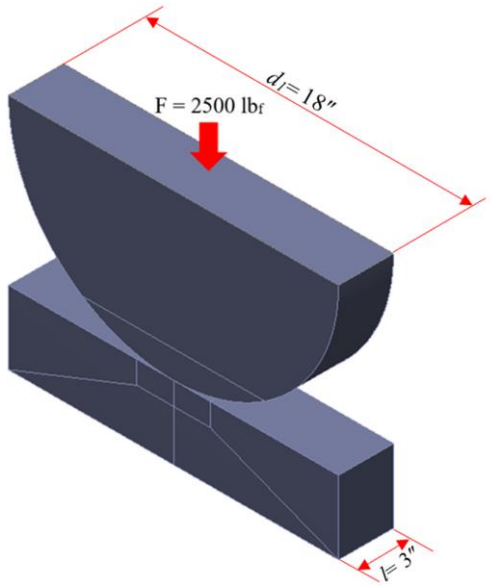

Figure 3.1 Profile for Hertz contact theory analysis

Table 3.1 Data used for Hertz contact theory

Description	Variable	Value	Unit
Force	F	2,500	lb_f
Length of contact	*l*	3	in.
Diameter of object 1 (Cylinder)	d_1	18	in.
Diameter of object 2 (Plane)	d_2		in.
Elastic modulus object1 (Cylinder)	E_1	29,000	ksi
Elastic modulus object2 (Plane)	E_2	29,000	ksi
Poisson's ratio object 1(Cylinder)	v_1	0.3	
Poisson's ratio object 2 (Plane)	v_2	0.3	

The results obtained from the Hertz contact theory between the cylinder and the plane surfaces include the half contact patch width (Equation 1), the maximum Hertz contact stress occurred at the center of the contact region (Equation 2), and the maximum stress in the cylinder along the x, y, and z-axis (Equations 3 to 5), respectively)Budynas & Nisbett, 2015(.

$$b = \sqrt{\frac{2F((1-v_1^2)/E_1 + (1-v_2^2)/E_2))}{\pi l\left(\frac{1}{d_1}+\frac{1}{d_2}\right)}} \quad (1)$$

$$p_{max} = \frac{2F}{\pi b l} \quad (2)$$

$$\sigma_{x,max} = -2vp_{max}\left(\sqrt{(1+\frac{z^2}{b^2})} - \left|\frac{z}{b}\right|\right) \quad (3)$$

$$\sigma_{y,max} = -p_{max}\left(\frac{1+2\frac{z^2}{b^2}}{\sqrt{(1+\frac{z^2}{b^2})}} - 2\left|\frac{z}{b}\right|\right) \quad (4)$$

$$\sigma_{z,max} = \frac{-p_{max}}{\sqrt{1+z^2/b^2}} \quad (5)$$

Where b=The half contact patch width (in.), F=Force (lb_f), v= ratio, E= Elastic modulus (ksi), d=Diameter (in.), p_{max}= The maximum Hertz contact Stress (ksi), l =Contact length (in.), $\sigma_{x,max}$ =Maximum principal stress along the x-axis (ksi), $\sigma_{y,max}$=Maximum principal stress along the y-axis (ksi), and $\sigma_{z,max}$=Maximum principal stress along the z-axis (ksi).

Table 3.2 lists the results calculated with Hertz contact theory from Equations 1 to 5. It is evident that the area of contact is a narrow rectangle of width (2b) equal 0.049 inches, the maximum Hertz contact stress (p_{max}) has an elliptical distribution across the contact region equal to 21.67 ksi, and the maximum stress along the x, y, and z axis are equal to 13 ksi, 21.67 ksi, and 21.67 ksi in compression, respectively.

Table 3.2 Result obtained in Hertz contact theory equation

Description	Variable	Value	Unit
Rectangular contact area width	2b	0.049	in.
Maximum Hertz contact stress	p_{max}	21.67	ksi
Maximum principal stress along the x-axis	$\sigma_{x,\,max}$	-13.00	ksi
Maximum principal stress along the y-axis	$\sigma_{y,\,max}$	-21.67	ksi
Maximum principal stress along the z-axis	$\sigma_{z,\,max}$	-21.67	ksi

Figure 3.2 shows the normalized stress from the center of the contact point to a distance of 3b (0.07 inch) below the depth of contact surface (z). In case of the shear stress, the maximum value occurs at z/b of 0.79 with a value of $0.3p_{max}$ or about 6.51 ksi.

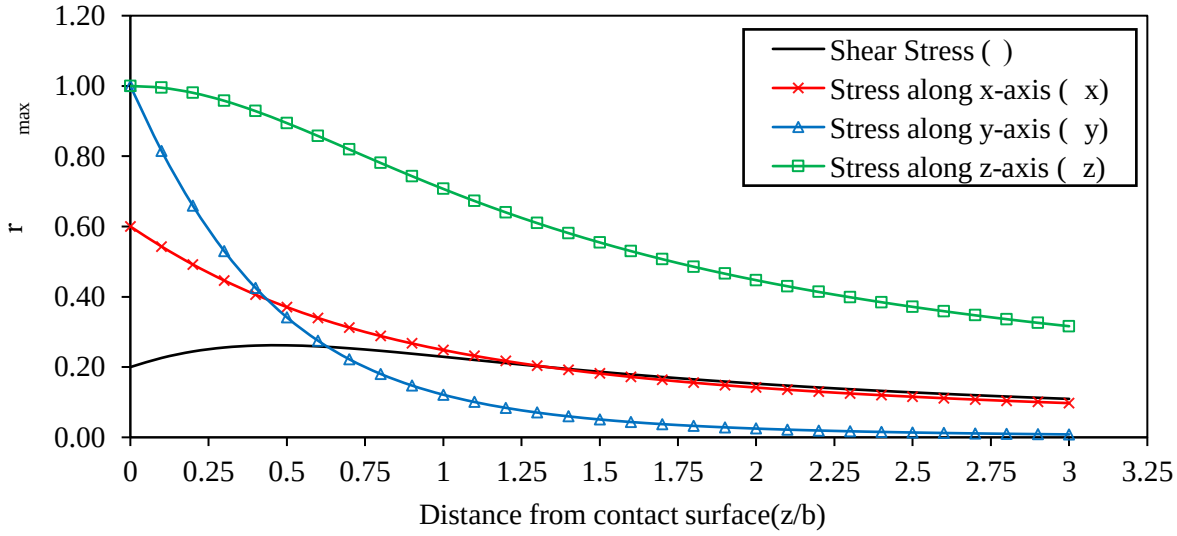

Figure 3.2 The absolute ratio between stress and maximum stress distribution

3.2 Numerical modeling for the Hertz contact theory

The contact region between cylinder and plane surface is a line for two parallel contact areas. Accordingly, nonlinear structural behavior can be created from contact nonlinearity, geometrical nonlinearity, and material nonlinearity. In this research, the contact stress analysis between cylinder and plane surfaces has nonlinearity using numerical modeling.

In contact problems, ANSYS® uses an incremental solution method, the Newton-Raphson, equilibrium-iteration procedure to analysis. The numerical modeling in ANSYS® performed to achieve accurate results with minimum computer processing time. Mesh refinement is one of significant procedures to improve reliable results. Meshing quality includes the need to check mesh density, aspect ratio and mesh style. Contact and material nonlinearities options are included in the numerical modeling in ANSYS®. In this study, a frictionless contact nonlinear option is used at the contact area between cylinder and plane surface. Sub-modeling is an additional technique for obtaining more accurate results focused on a specific area of the geometry that requires a finer mesh. This process of mesh refinement is crucial in approving numerical modeling by increasing reliable results.

As a preliminary study, a numerical modeling of a small scale cylindrical in contact with a plan was conducted to verify the Hertz contact theory. The small scale of the numerical modeling was created to minimize the simulation processing time for comparing with the theoretical from Hertz between the cylinder and plane surfaces. The dimension of the geometry and the applied force (F) of 2,500 lb_f, as shown in Figures 3.3.

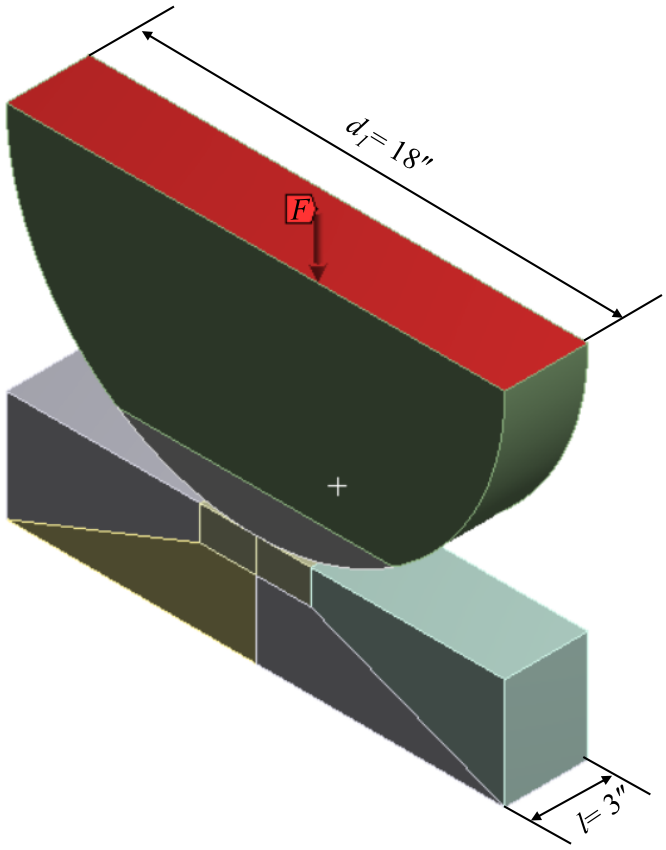

Figure 3.3 Geometry used for numerical modeling

3.3 Mesh generation for numerical modeling

One of the most significant tasks in numerical modeling is to generate a suitable mesh for the geometry. The reliable results with minimum data processing time and mesh creation require a proper mesh density and quality with well-shaped components. Too fine a mesh for the geometry and results with excessive data processing time and memory space, while too coarse a mesh might produce inaccurate results. Consequently, the mesh density and mesh style are important considerations for finite element mesh refinement. The proper meshing of the numerical modeling is an important step to consider since mesh styles control the accuracy, efficiency, and computer time.

Mesh refinement techniques are a suite of techniques that are commonly used in FEA software such as reducing the element size and increasing the element order. Reducing the element size is the original mesh refinement technique by reducing the element sizes throughout the geometry. Increasing the element order means to increase the number of divisions in the specific region by remeshing. Typically, mesh refinement is required in the area where higher stress-strain is expected. Furthermore, a coarse mesh could be applied to the less significant part of the geometry. Also, sub-modeling is another technique to develop the area with finer mesh. In this Hertz contact theory modeling validation mesh refinement was consider improving the numerical modeling results. The validity of the model with mesh refinement have to improve until the contact stress from numerical modeling differed from the Hertz contact theory less than one percent. The resulting mesh consists of at least 1,028,260 elements and 4,239,579 nodes.

The common mesh styles for three-dimensional modeling in FEA are tetrahedral and hexahedral shapes. A tetrahedral mesh does not have constraints in terms of component styles and a specified pattern generated to the numerical modeling, but unstructured tetrahedral meshing also requires more elements than a hexahedral dominant mesh)Shepherd & Johnson, 2006(. Typically, hexahedral meshes have some advantages over tetrahedral finite element meshes in terms of reduced error, smaller element numbers, and increased reliability)Shepherd & Johnson, 2006(. However, hexahedral finite element mesh generation has a limitation in terms of the geometry shape. The hexahedral mesh includes the pattern of the meshing and technically takes more effort to generate the style)Cifuentes & Kalbag, 1992(.

In this study, the hexahedral mesh generation for numerical modeling was preferred for Hertz contact theory modeling in ANSYS®, as illustrated in Figure 3.4.

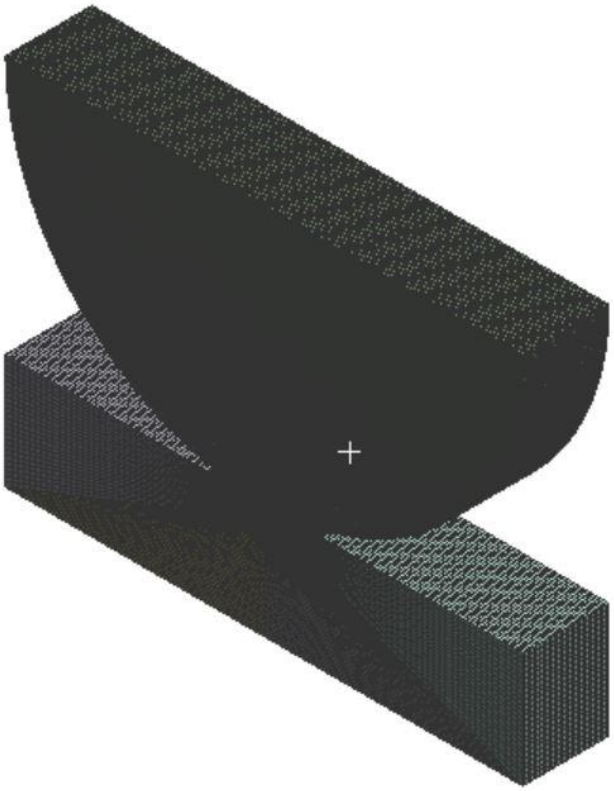

(a) Hexahedral mesh modeling

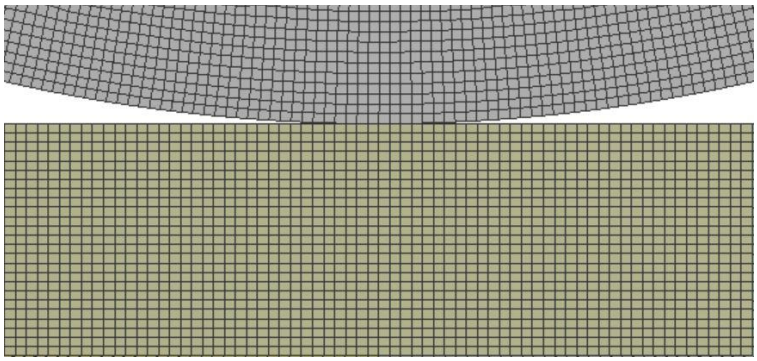

(b) Hexahedral mesh contact region

Figure 3.4 Hexahedral mesh

3.4 Contact in static structures

Hertz contact theory assumes that structures behave linearly and there is no friction in the contact surface. Two surface areas of geometry are frictionless for both Hertz contact theory and numerical modeling. Frictionless contacts types were used in this study to introduce contact nonlinearities between cylinder and plane surfaces)Lee, 2017(.

In ANSYS®, the frictionless contact is a nonlinear feature when two separate surfaces touch each other that are expected to interact with each other. One side of a contact pair is introduced as the contact part while the other surface is defined as the target part (see Figure 3.5). Typically, solid contact surfaces do not interpenetrate each other. Therefore, ANSYS® generates a relationship between two surfaces of the models to control them from penetration through each other during the simulation process. It can identify reasonable contact pairs by presenting contact parts (See Figure 3.5 (a)).

ANSYS® provides different contact pair elements, such as node-to-node, node-to-surface, and surface-to-surface. The contact area is loaded at the target surface where penetration is expected. Contact surfaces factor a wide range of types of interactions between elements in the geometry. In this research, surface-to-surface contact is used in the numerical modeling. The contact area of the cylinder is defined as a contact surface while the plane surface represents as a target surface (see Figure 3.5 (b)).

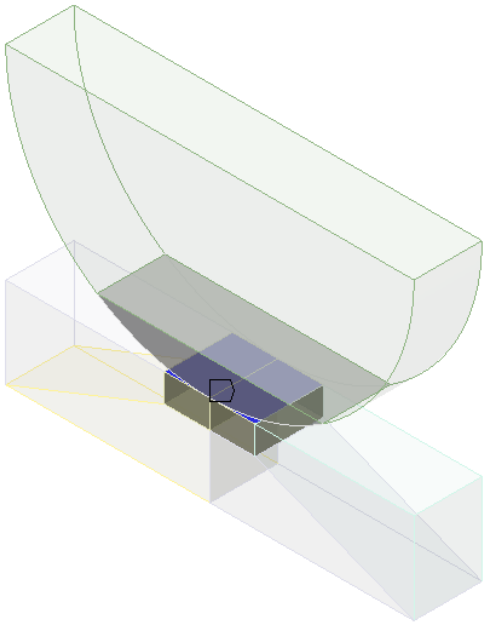

(a) Contact frictionless between cylinder and plane surface

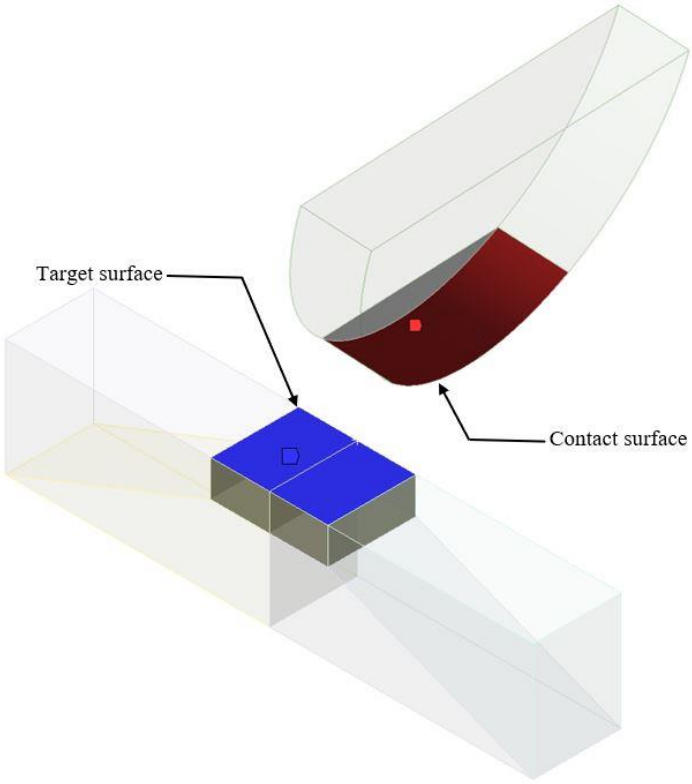

(b) Contact pair surface-to-surface between cylinder and plane surface

Figure 3.5 Contact modeling between cylinder and plane surface

3.5 Numerical modeling results

The contact stress of the numerical modeling is compared with the theoretical results from Hertz contact theory. High stresses were developed between the contact area between the cylinder and plane as shown in Figure 3.6. Table 3.3 summarizes and compares the maximum stresses between the numerical modeling and the Hertz contact theory. The difference between the theoretical result and numerical modeling is about 0.6% and 9.7% for the maximum contact stress and the maximum shear stress, respectively.

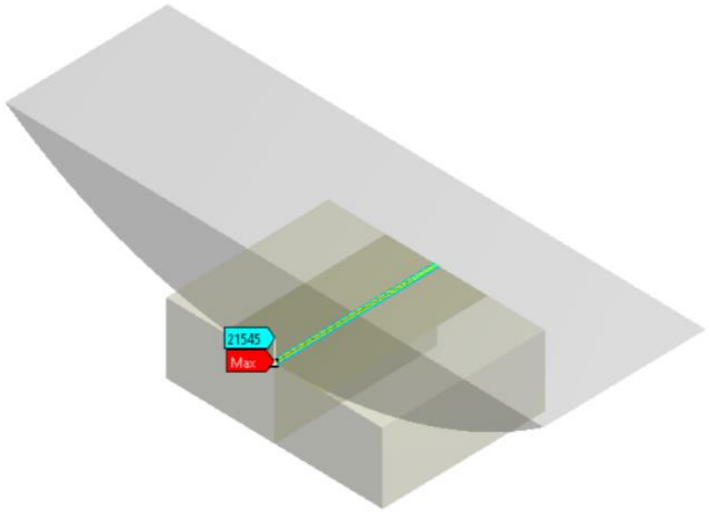

Figure 3.6 Contact stresses between cylinder and plane in the numerical modeling

Table 3.3 Contact stress comparison

Stress	**Hertz contact theory (ksi)**	**Numerical results (ksi)**	**Difference (%)**
Maximum contact stress	21.67	21.55	0.6
Maximum shear stress	6.51	7.14	9.7

CHAPTER 4. NUMERICAL MODELING COMPARING WITH FIELD DATA

The incremental launching method (ILM) is the one of the erection methods used for bridge construction in environmentally sensitive areas. This method is performed by constructing parts of the steel girders behind an abutment, linking them together, and pulling or pushing the assembled segments on support bearings to their permanent location. This chapter describes the validation between the field measurement and the numerical modeling.

4.1 Launching system description

The Iowa River Bridge (IRB) consists of four steel plate I-girders, each of which is approximately 11 ft deep and spans around 301 ft each over five spans over the Iowa River six piers)Wipf, et al., 2004(. To support the steel girders within the launch pit, four temporary rollers, notated in Figure 4.1 as R_A, R_B, R_C, and R_D, were installed behind Pier 6. The locations of the piers, 1 to 6, and plan view of the launching girders are illustrated in Figure 4.1 (a). The steel girders were arranged to start in a launching area located to east of Pier 6. The launching steel rollers with a diameter of 18 inches and a width of 6 inches were placed in the launch pit on the piers to reduce longitudinal resistance (see Figure 4.2). The temporary steel tapered launch nose attached to the two interior girders with a length of 146.5-ft. These nose parts were connected to two steel girders that were in vertical and longitudinal alignment with the two interior girders for the IRB. The nose assembly was used to control the launching girders upward over each pier (see Figure 4.3). The steel frame launching tail assembly is 24-ft long and temporarily connected to the end of launching girder, as shown in Figure 4.4)Wipf, et al., 2004(.

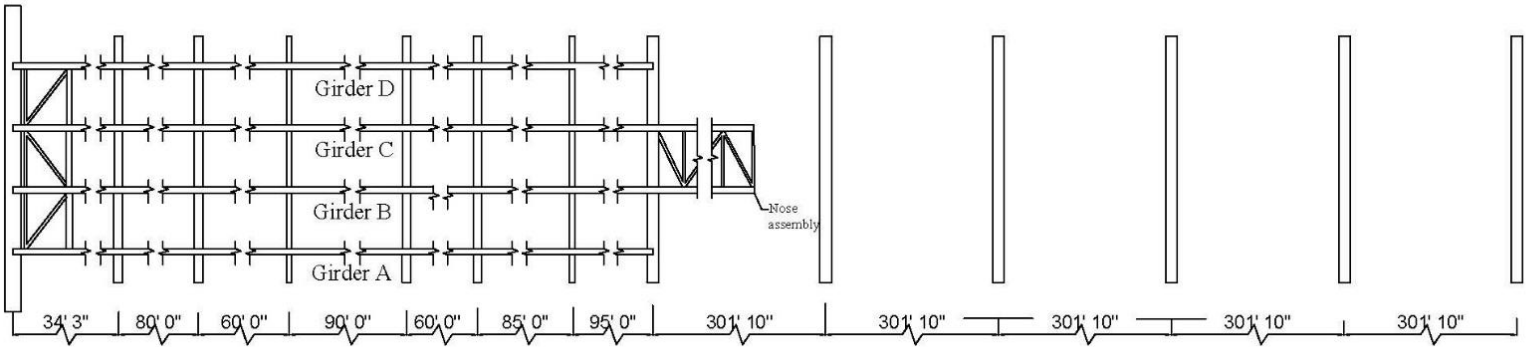

(a) Plan view of girders

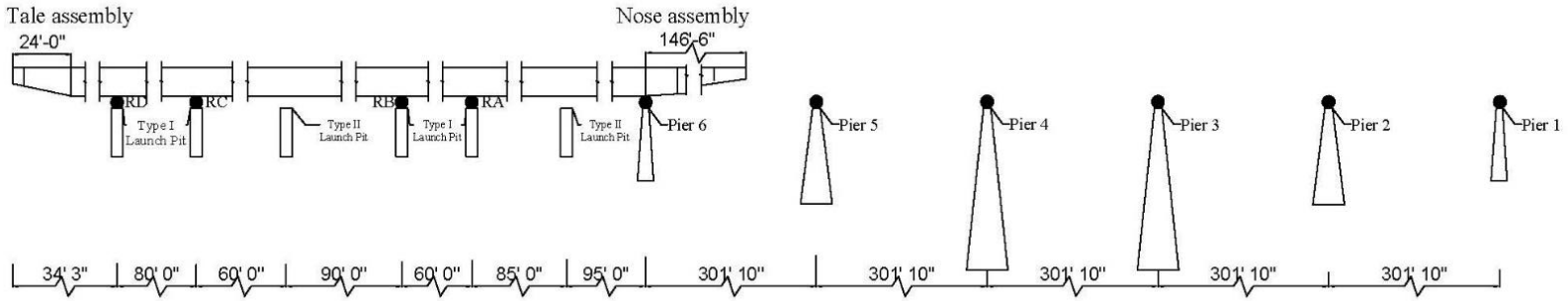

(b) Elevation view of girders

[redacted]

Figure 4.2 Steel roller support during launching)Wipf, et al., 2004(

Figure 4.3 Tapered launching nose leading)Wipf, et al., 2004(

Figure 4.4 Launching tail including transverse jacking beam)Wipf, et al., 2004(

The detailed elevation views of the girder during Launch 3 (from launching distance 794 to 854 ft) are illustrated in Figure 4.5. Contact-strain data were collected during Launch 3 of the westbound roadway of the IRB Girder C (an interior girder). The instrumentation was installed on the cross-section at the point of highest contact stress, where it passed over Pier 6, as shown in Figure 4.5 (b))Wipf, et al., 2004(. In this study, the launching stage of the IRB girder C at 823.5 ft was studied and the strain measurement at this stage was compared with the numerical modeling performed for this study.

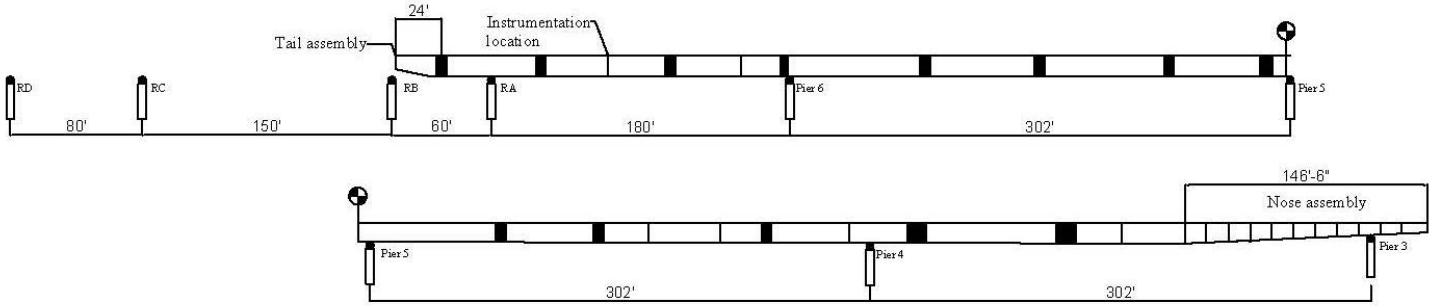

[redacted]

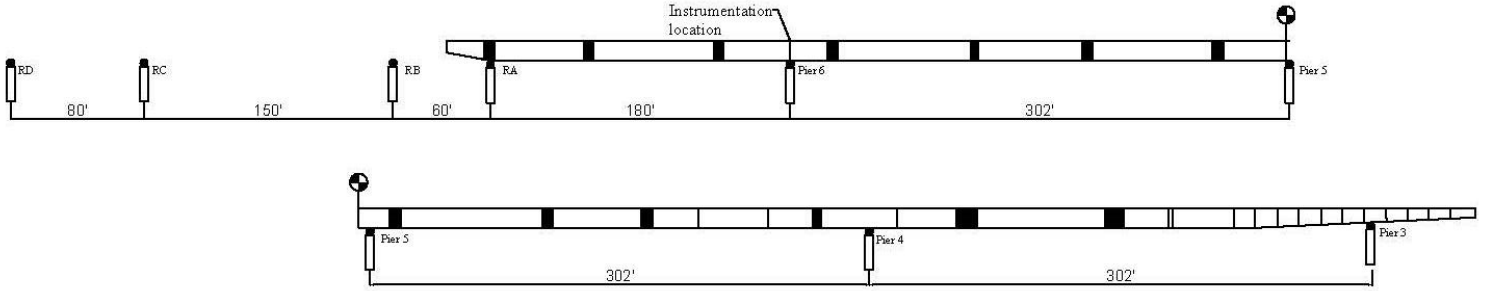

(b) Launch distance 824 ft

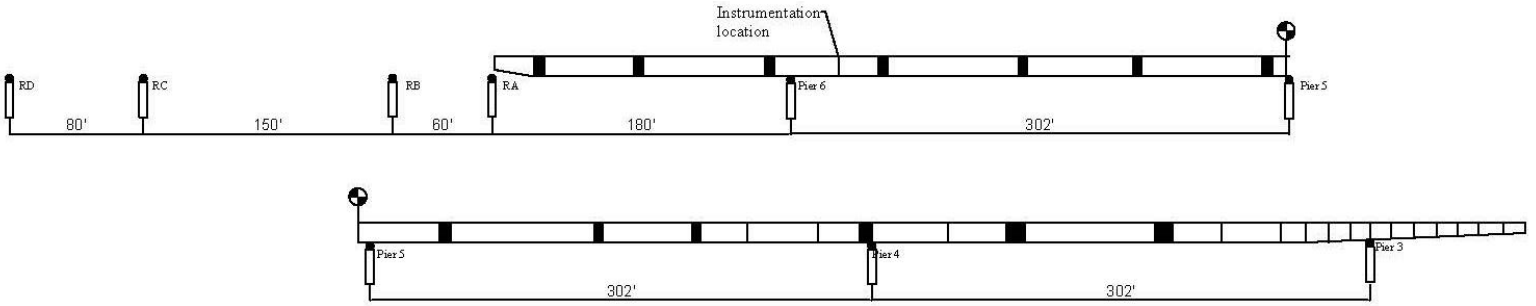

[redacted]

[redacted]

4.2 Numerical modeling of Iowa River Bridge (IRB)

The cross section of the IRB Girder C has a web of 135-7/8 inches by 7/8 inches, top flange of 14-3/4 inches by 7/8 inches, and a bottom flange of 19-5/8 inches by 1-1/4 inches (see Figure 4.6). The total of 13 strain gages were installed on the lower parts of the Girders C. The strain gage system names represent a specific point on the girder. For example, CS describes Girder C and Southern side, CN describes Girder C and Northern side, BW represents Bottom gages, MW represents Middle gages, and TW represents Top gages on the Web, IF represents Inner gages and OF represents Outer gages on the Top surface of the bottom Flange, OBF represents Outer gages, and CB represents Center gages on the Bottom surface of the bottom Flange of Girder C (see Figure 4.7). Moreover, the lower surface of the girder bottom flange was in contact with the roller support surface. The dimension of the roller support IRB Girder C is a diameter of 18 inches and a width of 6 inches. The strain data were recorded every 0.25 second during the field measurement.

The numerical modeling includes geometry and material properties, the girder-aspect ratio, member end forces, mesh generation, contact nonlinearity, and numerical modeling settings. The following assumptions were made: the girder cross-section was held constant, only static loads from self-weight are included, and the steel roller is supported at the center of the steel girder during launching.

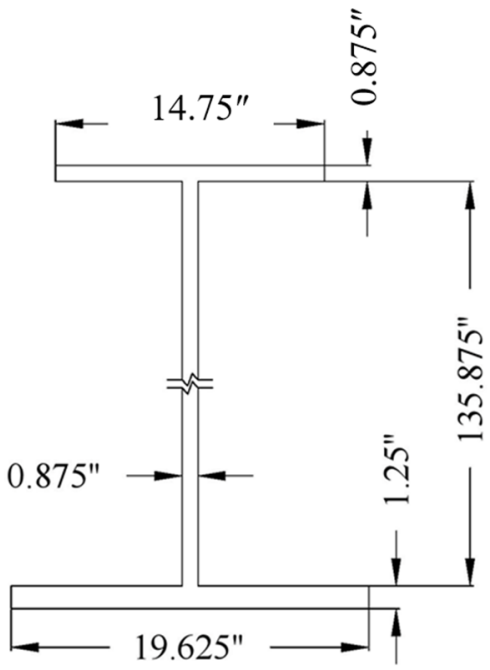

Figure 4.6 Girder C cross-section

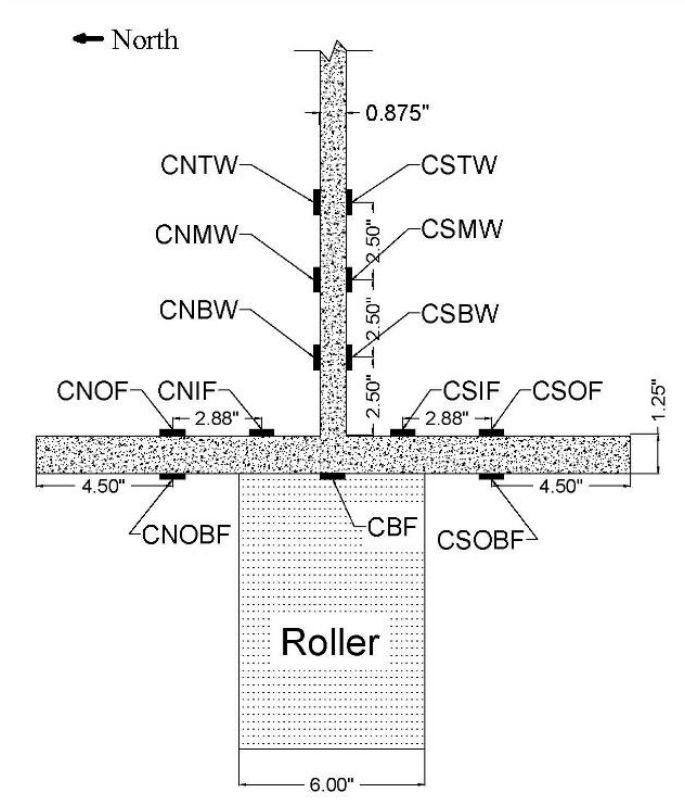

Figure 4.7 Strain gage positions

4.2.1 Geometry and material properties

The numerical modeling considered a symmetricity of the bridge I-girder. The geometry and material properties were set to compare with the field measurement from IRB Girder C. Since the IRB Girder C is symmetric in terms of geometry, load, and constraints, the numerical modeling reduces the size of geometry and complexity of the model by modeling only half of the section as shown in Figures 4.8. The contact-pair concept was applied between the surface of the roller and the lower surface of the bottom flange. The material properties for the selected element are those of steel: density of 490 lb/ft^3, a modulus of elasticity of 29,000 ksi, a yield strength of 50 ksi and 36 ksi for the girder and the roller, respectively, and a ratio of 0.3)Chang, 2004(.

(a) Isometric view of girder

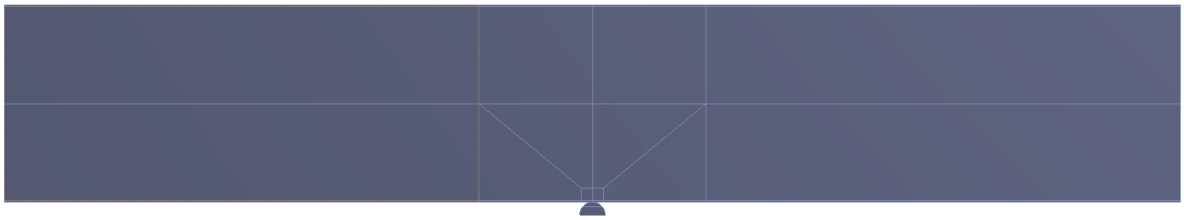

(b) Front view of girder

Figure 4.8 IRB Girder C geometry

(c) Side view of girder

Figure 4.8 Continued

4.2.2 Girder-aspect ratio

Elementary-beam theory assumes the length of a span is significantly larger than the depth of section. Since the entire girder is too large to analyze in three-dimensional modeling, only portion of girder was analyzed. A deep beam defines a beam with a short shear span with a girder- r (rd r . d) 2)Holmes & Mason, 1972(. According to d (2004), the most effective girder-aspect ratio in the analysis was determined to be 6. The girder-aspect ratio defines the ratio between the length and depth of the girder. Once the most effective girder-aspect ratio is determined, the member-end forces from a simple beam analysis need to apply to the three-dimensional model since modeling of the entire bridge is not desirable for FEA.

Figure 4.9 illustrates the concept of the girder-end forces on a portion of the bridge girder. In this figure, the following notation is used: n = Girder aspect ratio, d = Girder depth, n·d = Analyzed girder length, V_L = Shear force on the left end, V_R = Shear force on the right end, M_L = Bending moment on the left end, and M_R = Bending moment on the right end.

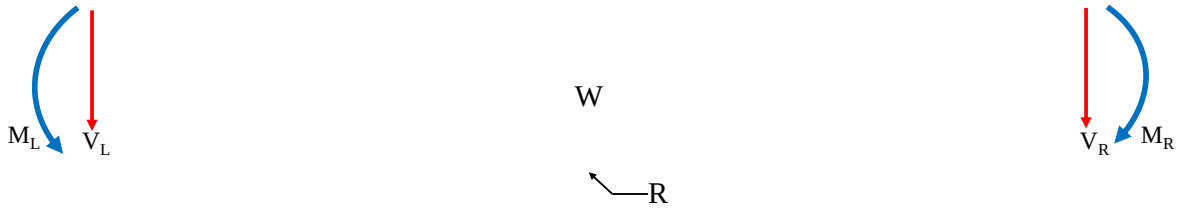

Figure 4.9 Girder segment used for the contact-stress analysis

4.2.3 Member end forces

The member-end forces at both end sections were obtained using a simple beam (line) analysis in STAAD Pro®. For simplicity, the nose and tail assemblies were assumed to be half weight of Girder C in the beam analysis. Figure 4.10 illustrates the structural behavior and internal forces at stage of 823.5 ft when the instrumented section was directly positioned over the roller at Pier 6.

Shear force and bending moment were collected at 34.5 ft away from Pier 6 at the left and right ends (see Figure 4.10 (c) and (d)) were applied to the numerical modeling in ANSYS® (see Table 4.1).

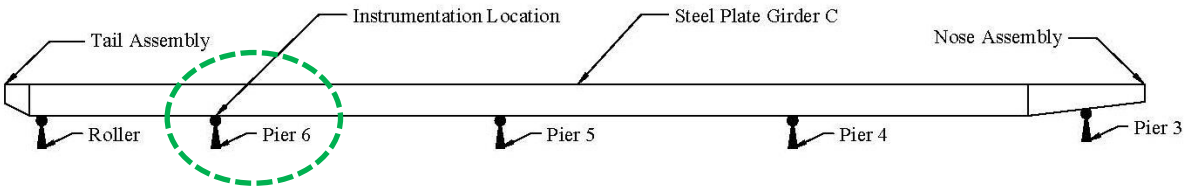

(a) Configuration

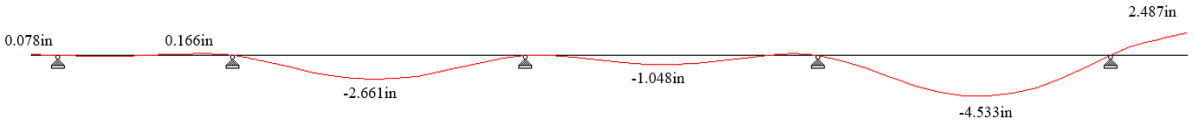

(b) Deflection shape

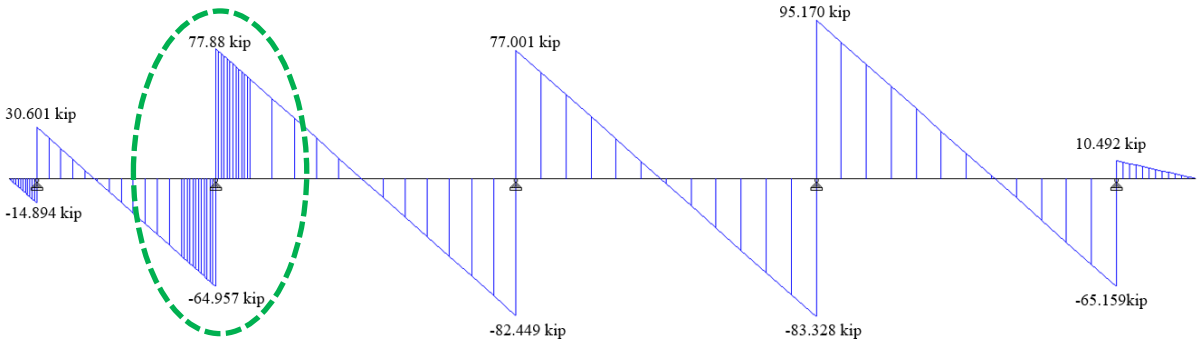

(c) Shear diagram (F_y)

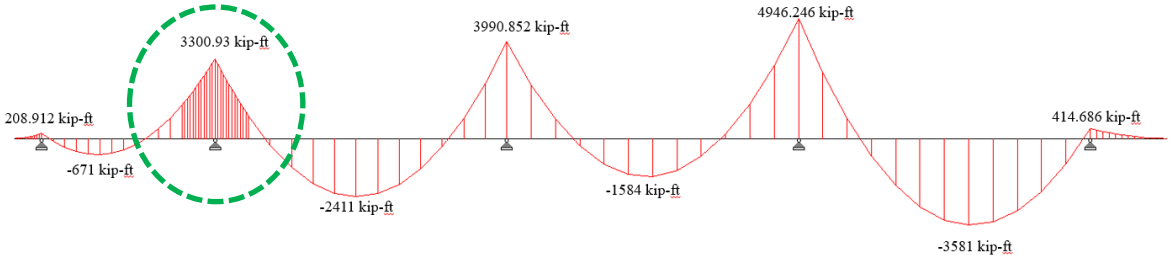

(d) Bending moment diagram (M_z)

Figure 4.10 Line analysis of Girder C at stage 823.5 ft

Table 4.1 IRB Girder C member-end forces

Girder-aspect ratio	6	
Member-end Forces	Left end	Right end
Bending moment (kip-ft)	-1,375.87	-930.02
Shear force (kips)	-46.64	59.56

4.2.4 Mesh generation

The hexahedral mesh can be generated for the complex geometries in finite element analysis. In addition, mesh density between contact areas is found to influence the reliable results of the numerical modeling directly. To standardize the contact area analysis, mesh with a small element size for all the configurations are chosen. The use of hexahedron elements can reduce the time needed to generate the mesh, which has the advantages in terms of reducing the number of elements and reliability improvement (Shepherd & Johnson, 2006). In the modeling, the hexahedral mesh was generated with the high density around the contact area between the lower surface of the bottom flange and roller, which is significant for achieving accurate contact strain results and minimizes computational processing time. For this study, the numerical modeling has a total of 2,299,747 nodes and 506,994 elements. The minimum mesh size at web interface and the flange of the Girder C were approximately 0.1 inches, which have a direct influence on the reliable of the solutions, as shown in Figures 4.11.

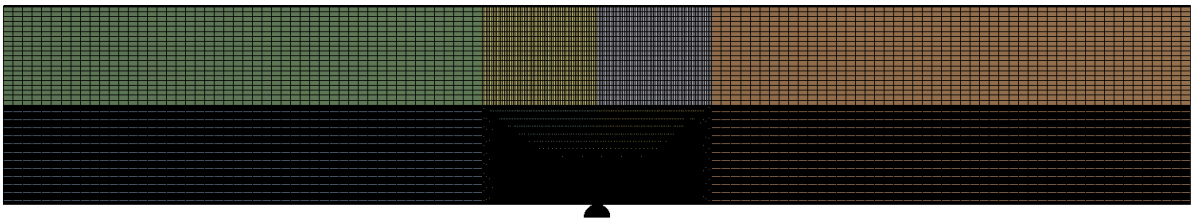

(a) Model with hexahedral mesh

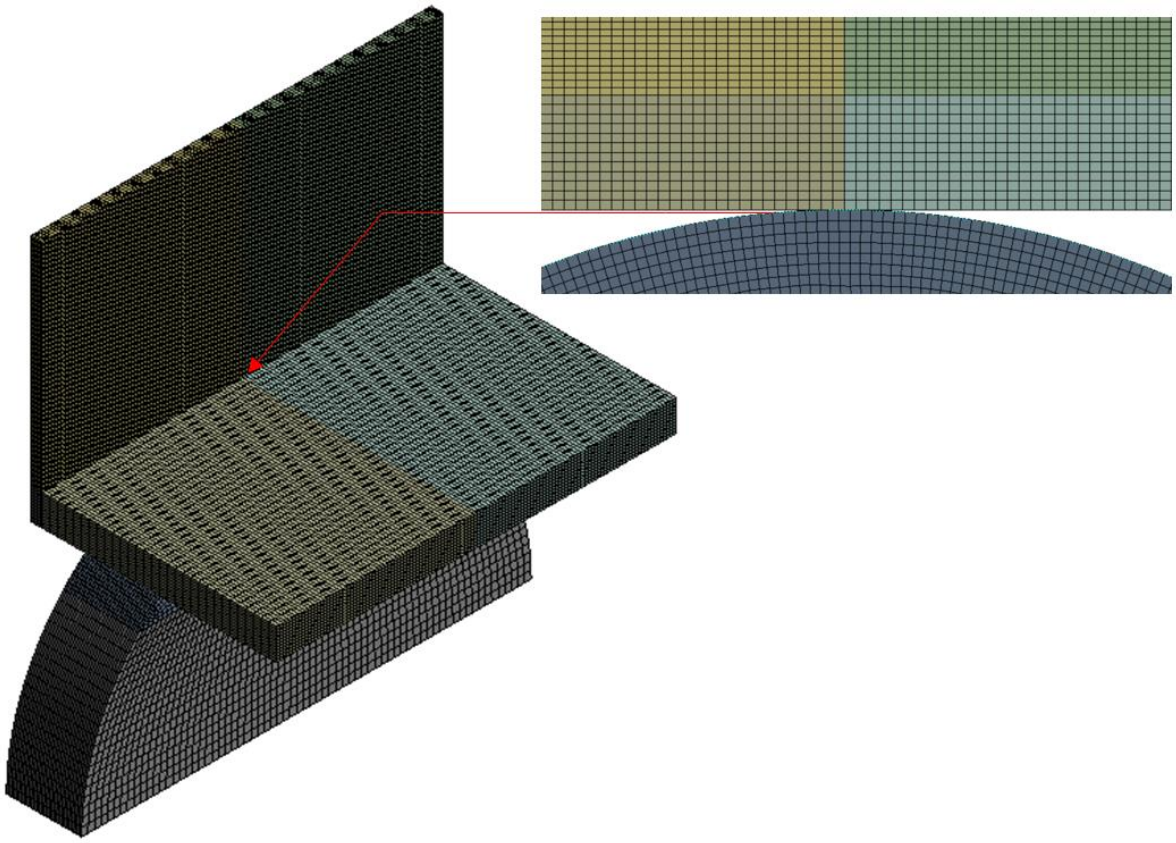

(b) Hexahedral mesh around the contact area

Figure 4.11 Hexahedral mesh modeling of the IRB Girder C

4.2.5 Contact nonlinearity

The frictional contact surface-to-surface was applied between contact surfaces because contact type introduces contact nonlinearities in ANSYS®. Contact problems caused two significant difficulties during the simulation. First, the areas of contact (i.e., size, location, shape, etc.) are commonly unknown until the problem has been solved. Second, the solution is dependent on the load, material, boundary conditions, and other factors (refer to section 3.4. for details about contact in static structure).

The specified contact surfaces for the IRB Girder C contact modeling (the original modeling) is illustrated in Figure 4.12. Half of the lower surface of the bottom flange was defined as a target surface, and the half of the roller surface was defined as a contact surface. The friction contact between surfaces was applied to the numerical modeling with a friction coefficient of 0.3.

Figure 4.12 View of contact surface in the IRB Girder C contact modeling

4.2.6 Numerical modeling settings

Shear force and bending moment were collected at 34.5 ft away from the Pier 6 in left and right by considering a girder-aspect ratio of 6)Chang, 2004(. As discussed earlier, the half value of the shear forces (V_L = -46.64 kips, V_R = 59.56 kips) and bending moments (M_L = -1375.87 kip ft, M_R = -930.02 kip ft) were applied as the member-end forces to both sides due to symmetric geometries. Also, the self-weight (W) of the steel girder and roller was considered in the modeling. The boundary condition for this analysis is a fixed support that was applied at the bottom surface of the half roller (R), as shown in Figure 4.13.

The total solution time required for numerical modeling approximately 6 hours for the r d r -7700 (CPU@ 3.6 GHz and RAM capacity of 32 GB) as a reference.

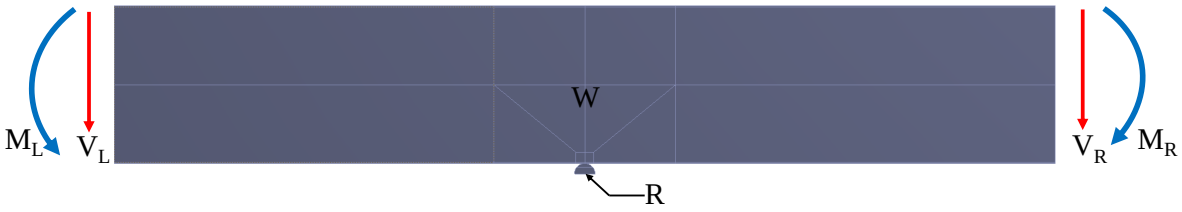

Figure 4.13 Structural analysis settings for IRB Girder C

4.3 Numerical modeling results

Since there are several strain gages installed to measure the contact strain during the launch of the IRB)Wipf, et al., 2004(. The selected vertical strains on the web and longitudinal strain on the bottom flange of the IRB Girder C were compared with the IRB Girder C contact modeling near Pier 6 at stages from 823 ft to 824 ft.

4.3.1 Web

The numerical modeling of vertical strain in the web of Girders C located near Pier 6 is shown in Figures 4.14 and 4.15, respectively. As shown in the figures, the numerical modeling results illustrate a similar pattern to the field measurement. Figures 4.14 presents the vertical strain in the lower portion of the web plate of Girder C near Pier 6. The numerical modeling results from ANSYS follow a similar pattern strain measured above the bottom surface of the bottom flange from 1.25 inches to 10 inches between the launch stage 823 and 824. Moreover, Figure 4.15 shows the vertical strain in the web plate of the Girder C at CBW, CMW, and CTW near Pier 6. The predicted strains illustrated in the figure also showed a similar pattern to the field data. The predicteded strains from ANSYS at CBW, CMW, CTW differed from the field measurement about 6%,10%, and 14%, respectively.

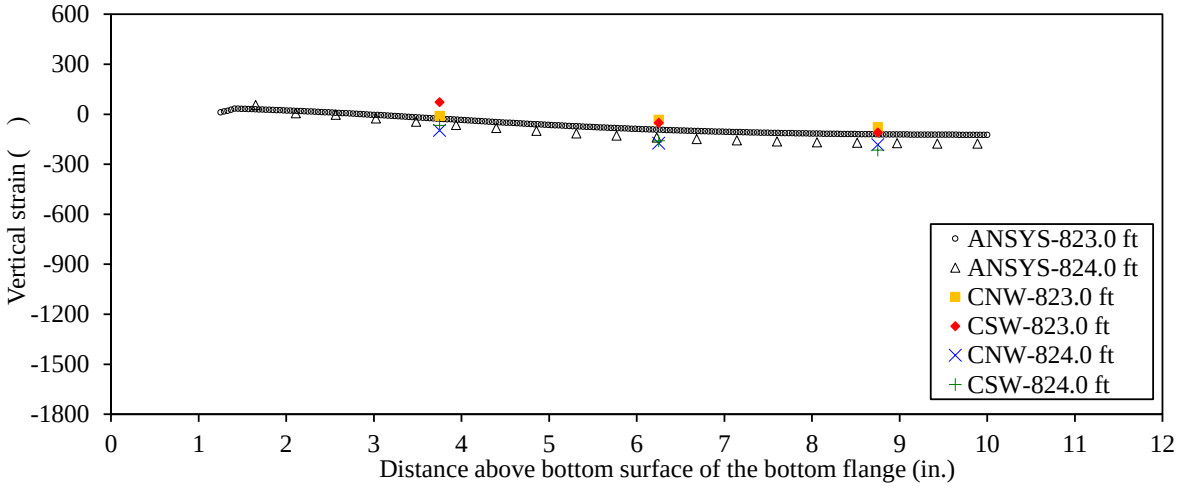

(a) Launch distance at 823.0 ft and 824.0 ft

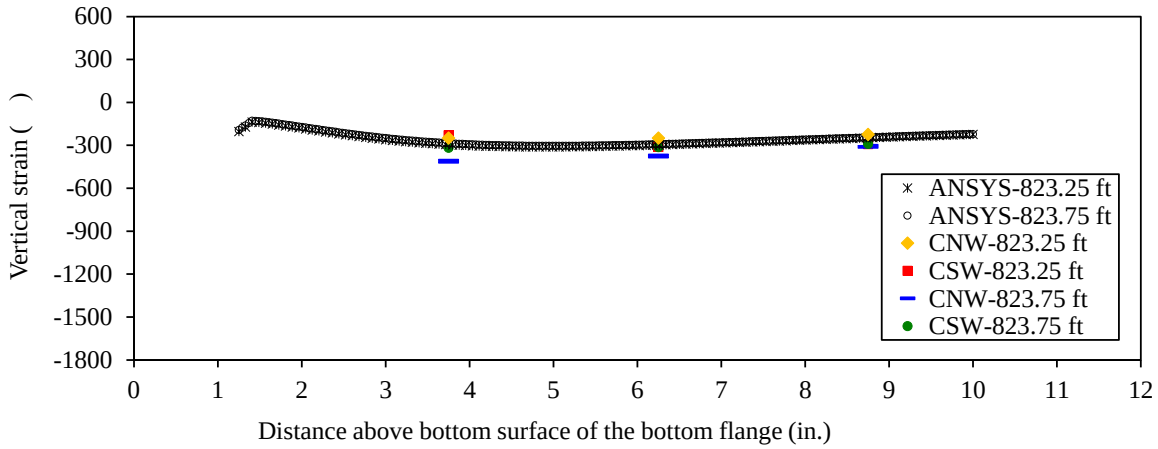

(b) Launch distance at 823.25 ft and 823.75 ft

Figure 4.14 Vertical strain in the web of Girder C near Pier 6

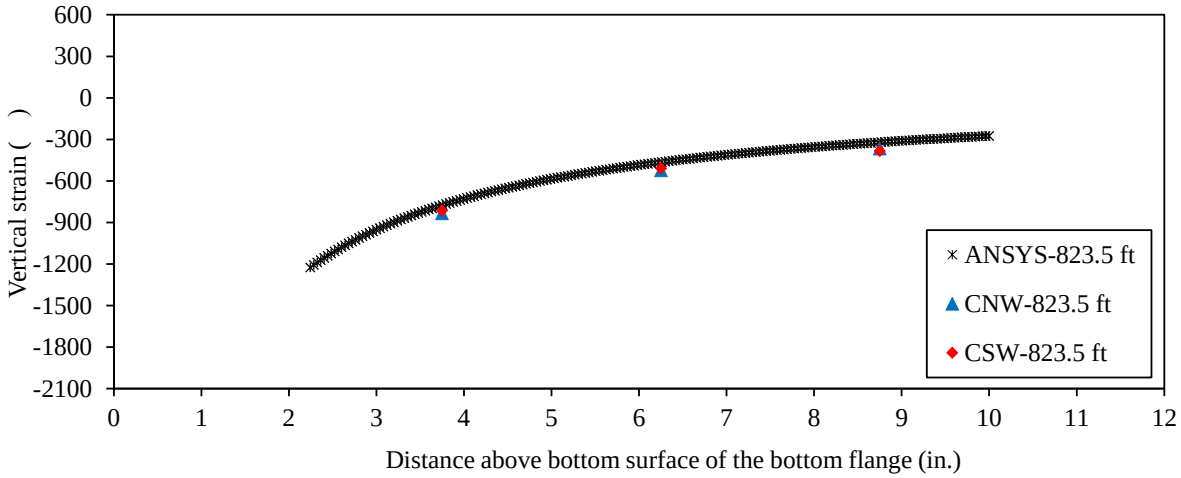

(c) Launch distance at 823.5 ft

Figure 4.14 Continued

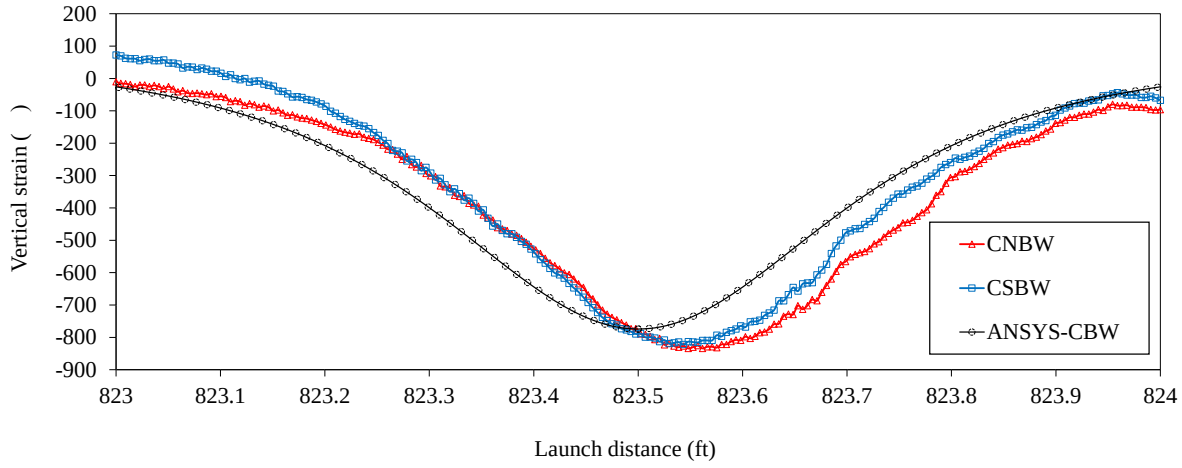

(a) From bottom portion gages

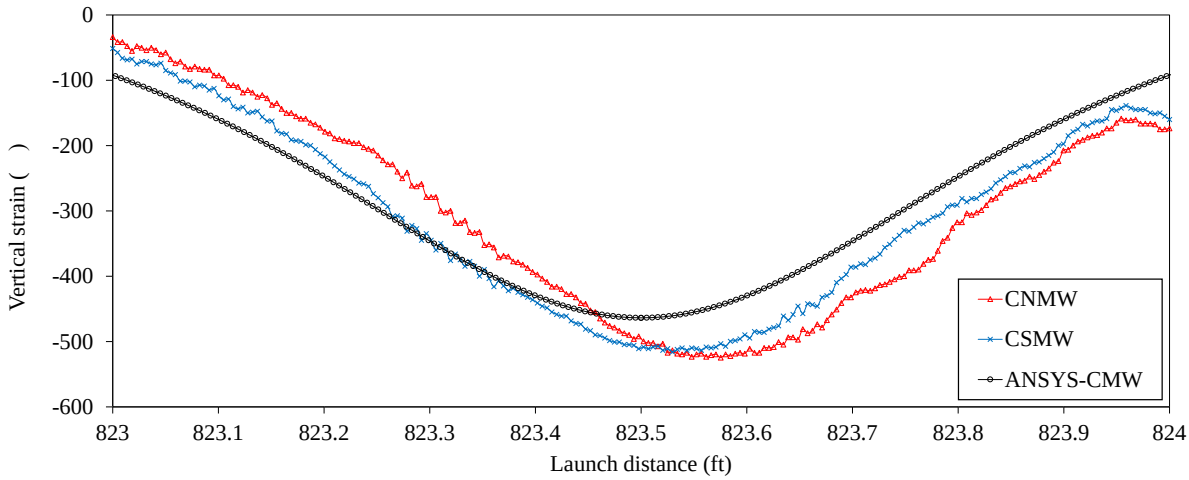

(b) From middle portion gages

Figure 4.15 Vertical strain in the web of Girder C from 823 ft to 824 ft

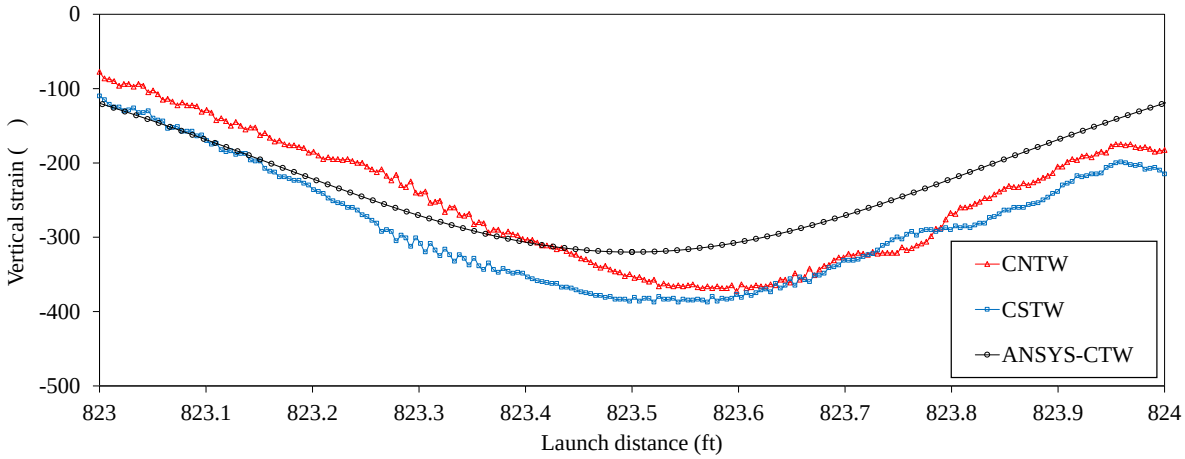

(c) From top portion gages

Figure 4.15 Continued

4.3.2 Bottom flange

In the numerical modeling, the predicted longitudinal strains at the lower surface of the bottom flange of the IRB Girder C were compared with the field measurement on the outer strain gage of the bottom flange (COBF) and the center strain gage of the bottom flange (CBF), as shown in Figure 4.16. The predicted longitudinal strain at COBF from 823 ft to 824 ft collected by ANSYS® followed a similar pattern of the field data (see Figure 4.16 (a)).

On the other hand, the strain value of CBF at the stage of 823.5 ft from the field data increases up to 4390 micro-strains (με) in compression while the corresponding numerical modeling shows approximately 2870 με (see Figure 4.16 (b)). The strain values measured from CBF could be a combination of the flange strain and gage strain itself due to the excessive pressure by the roller. Or the extreme strain data from the CBF could be measured beyond stage 823.5 ft due to the gages being destroyed when they encountered the roller)Chang, 2004(. In ANSYS®, the maximum strain occurred 0.22 inches away from the center of the contact point. The value increases up to 4252.4 με (compression) that was difference 3% from the field collected data at CBF, as shown in Figure 4.17 (b). This comparison reveals the significance of numerical modeling for contract stress.

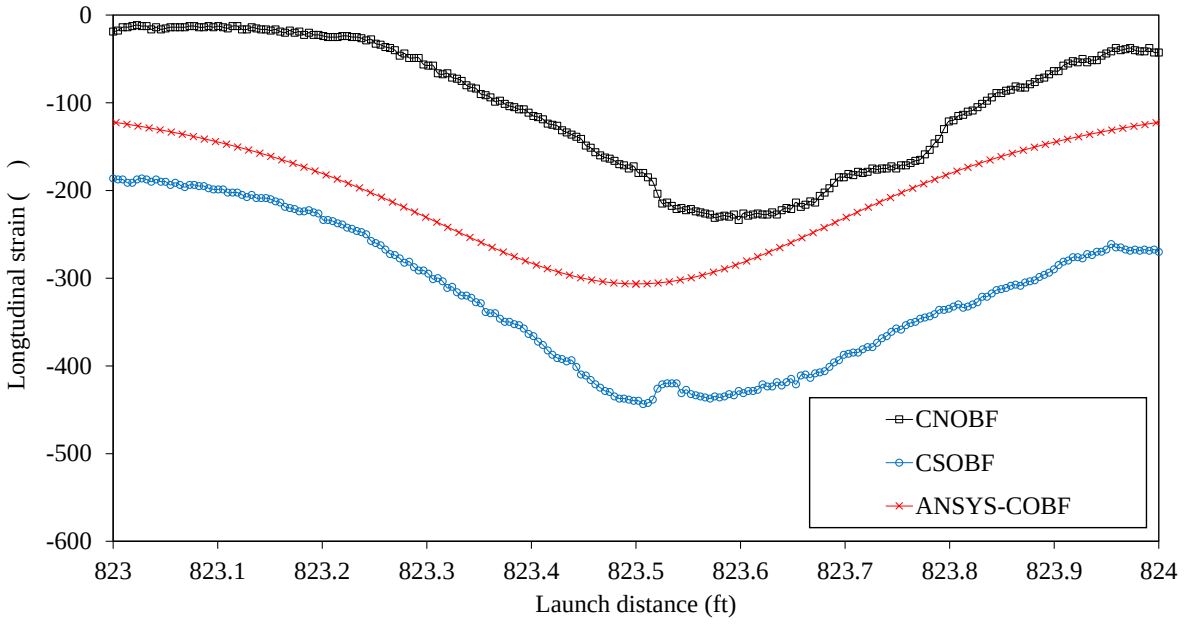

(a) Longitudinal strain at the outer strain gage of the bottom flange (COBF) from 823 ft to 824 ft

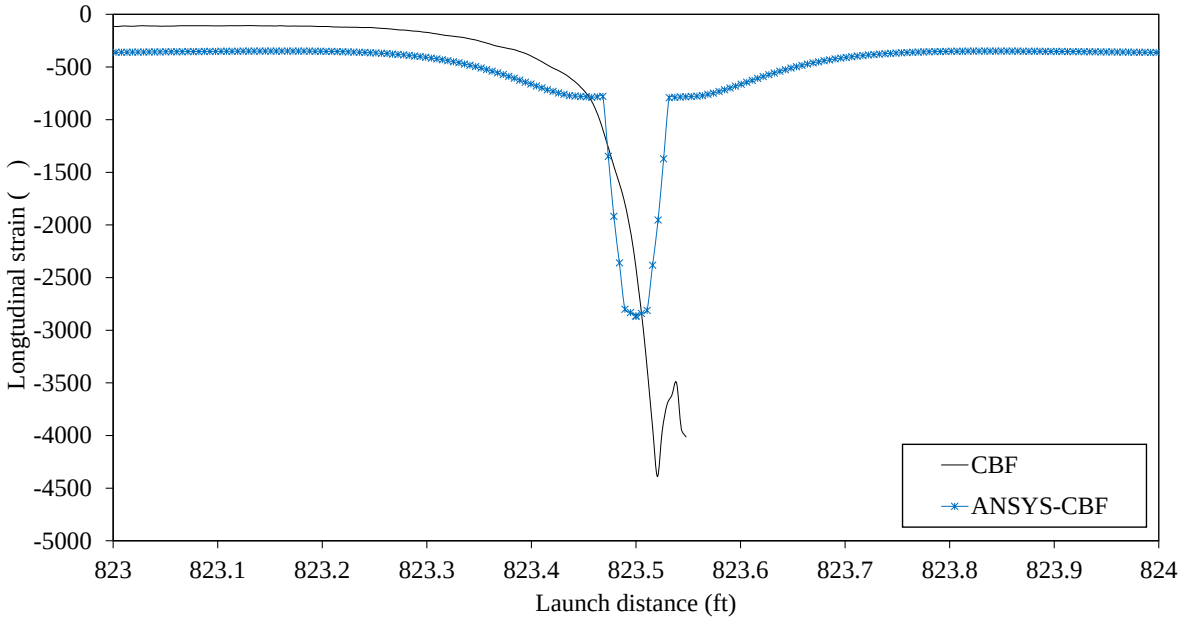

(b) Longitudinal strain at the center strain gage of the bottom flange (CBF) from 823 ft to 824 ft

Figure 4.16 Longitudinal strain at the bottom flange from 823 ft to 824 ft

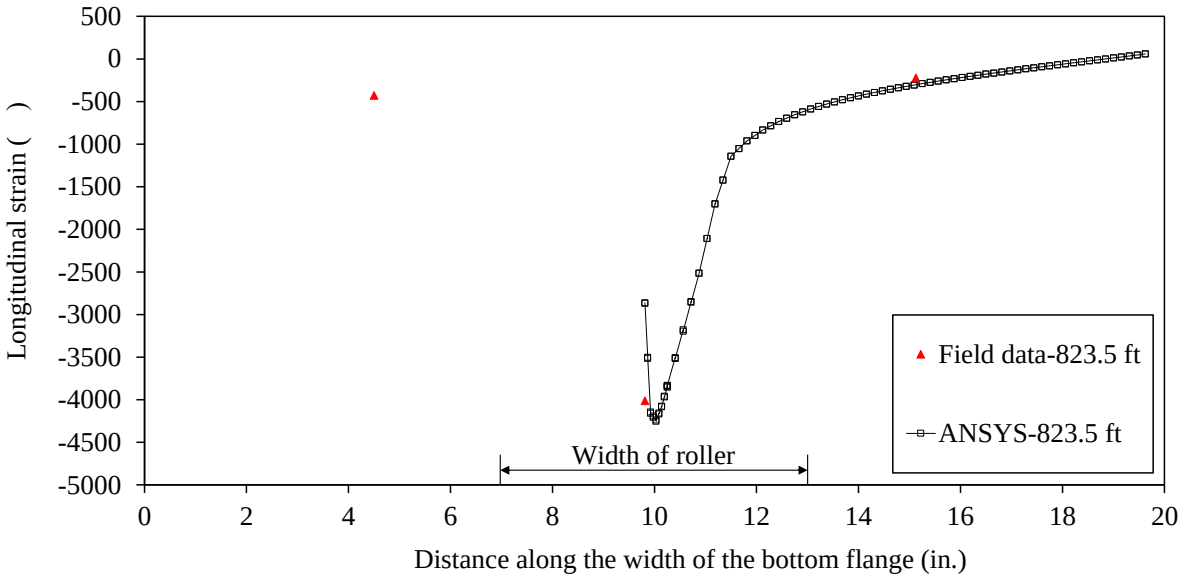

(a) Longitudinal strain in lower surface along the width of bottom flange

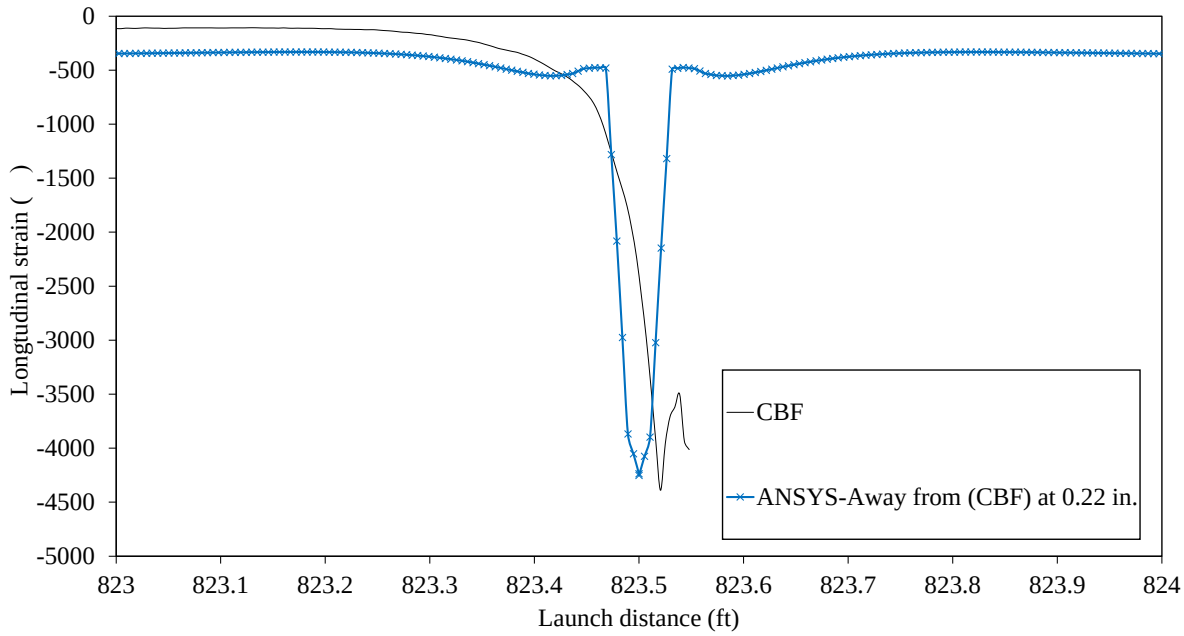

(b) Longitudinal strain away from the middle strain gage (CBF) at 0.22 inches

Figure 4.17 Longitudinal strain of the bottom flange near Pier 6

CHAPTER 5. SIMPLIFIED CONTACT MODELING

Since the internal forces vary depending on the girder stage, it is not easy to modify the input data in the numerical modeling each analysis. In addition, according to the Hertz contact theory, the most significant factor in contract stress is the vertical force. Thus, the numerical modeling for the IRB contact stress was simplified and the results were compared with the previous numerical modeling and the field data again. The following assumptions toward the simplified modeling are considered: the only portion of the girder is considered with a girder aspect ratio of 6, the model is symmetric in loading, geometry, and boundary conditions, the roller is positioned at the center of the girder bottom flange, and only roller reaction impact the contact stress significantly while bending moment is ignored.

Similarly, half of the roller surface is modeled as a contact surface and half of the lower surface of the bottom flange can be defined as a target surface. The contact friction of 0.3 is applied between the contact surfaces. However, the reaction from the previous modeling including both end shear forces, and self-weight were applied at the bottom of roller in the simplified contact modeling. The boundary condition in the modeling includes fixed top surface of the top flange.

5.1 Geometry and material properties

Figure 5.1 illustrates the girder segment used to be an initial modeling for the analysis of the different parametric parameters of this dissertation. Since the IRB contact model is symmetric in the transverse direction, with load conditions, and expected deformation of the structure, one half of the girder and the roller were modeled. Flanges and web were created and then merged to each other in a similar way described in Chapter 4. The contact-pair concept with friction coefficient of 0.3 was applied to the contact of geometry between the

surface of the roller and the lower surface of the bottom flange. The material properties for the modeling is a structural steel with a density of 490 lb/ft^3, a modulus of elasticity of 29,000 ksi,

d r 0. .

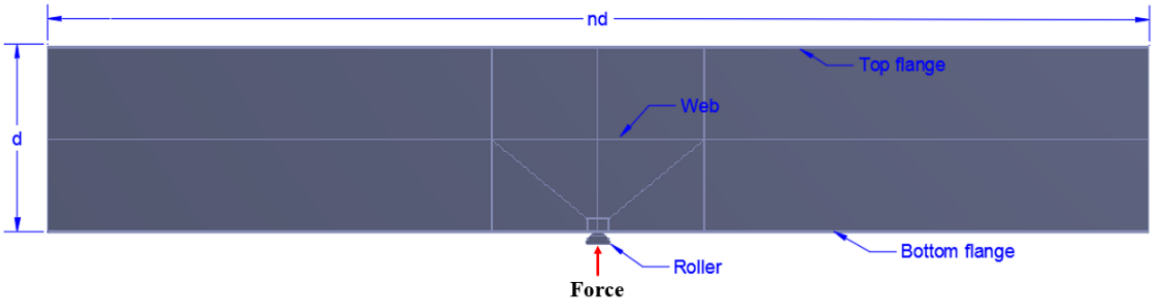

Figure 5.1 Girder segment used for analysis several parametric studies

5.2 The modeling approach for simplified modeling

The simulation for the contact stress for the parametric study commonly requires a smaller element size near the contact region between two solid surfaces than the region far away from where the contact occurs. However, smaller element sizes increase the number of elements and computational processing time for simulation. The dimension for concentration parts with fine mesh can be seen in Figure 5.2 (a). The density of 0.1 inches uses hexahedral mesh to validate the results from modeling for parametric study around the contact area while a coarser mesh is defined in the less significant regions of interest due to limited computer resource (see Figure 5.2 (b)), and the number of nodes and elements of a hexahedral mesh are 2,299,747 and 506,994, respectively.

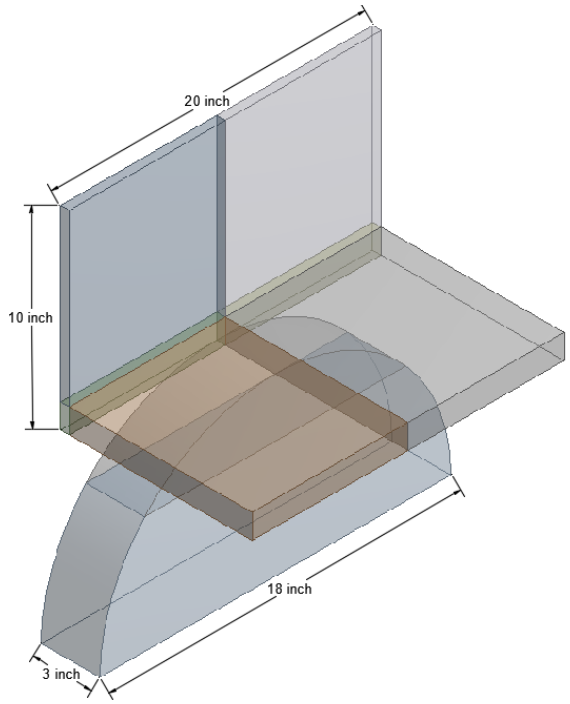

(a) Geometry

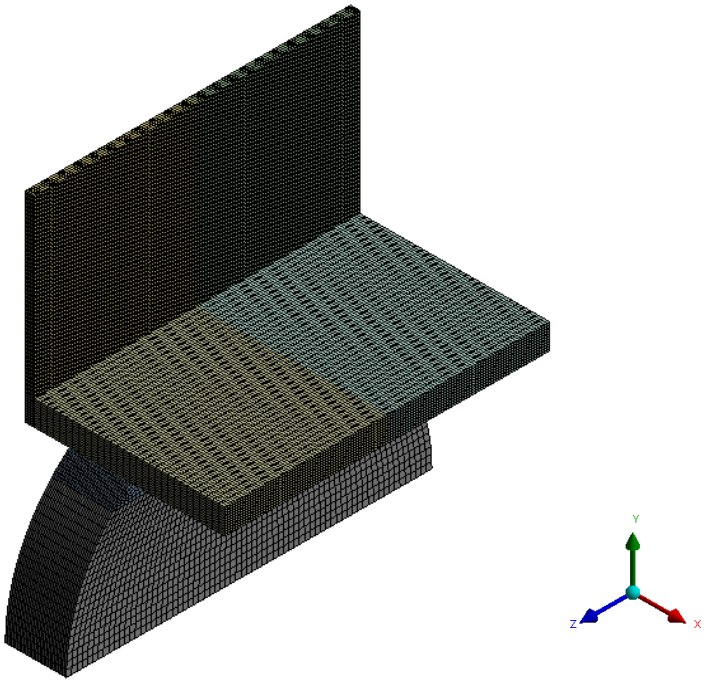

(b) Hexahedral Mesh

Figure 5.2 The concentration parts

In the modeling, hexahedral mesh was used. The force was applied at the bottom surface of the roller. The top surface of the top flange is fixed as shown in Figure 5.3. The geometry and load are from the IRB line analysis with a girder-aspect ratio of 6.

Figure 5.3 Structural analysis settings

Since the geometry, boundary condition, and load are symmetric, half of the roller surface is modeled as a contact surface (see Figure 5.4 (a)), and half of the lower surface of the bottom flange can be defined as a target surface (see Figure 5.4(b)), respectively. The contact friction of 0.3 is applied between the contact surfaces. The solution time required approximately 2 hours while the initial modeling required approximately 6 hours with a same computer specification.

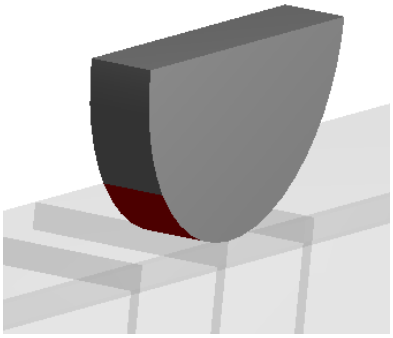

(a) Contact surface

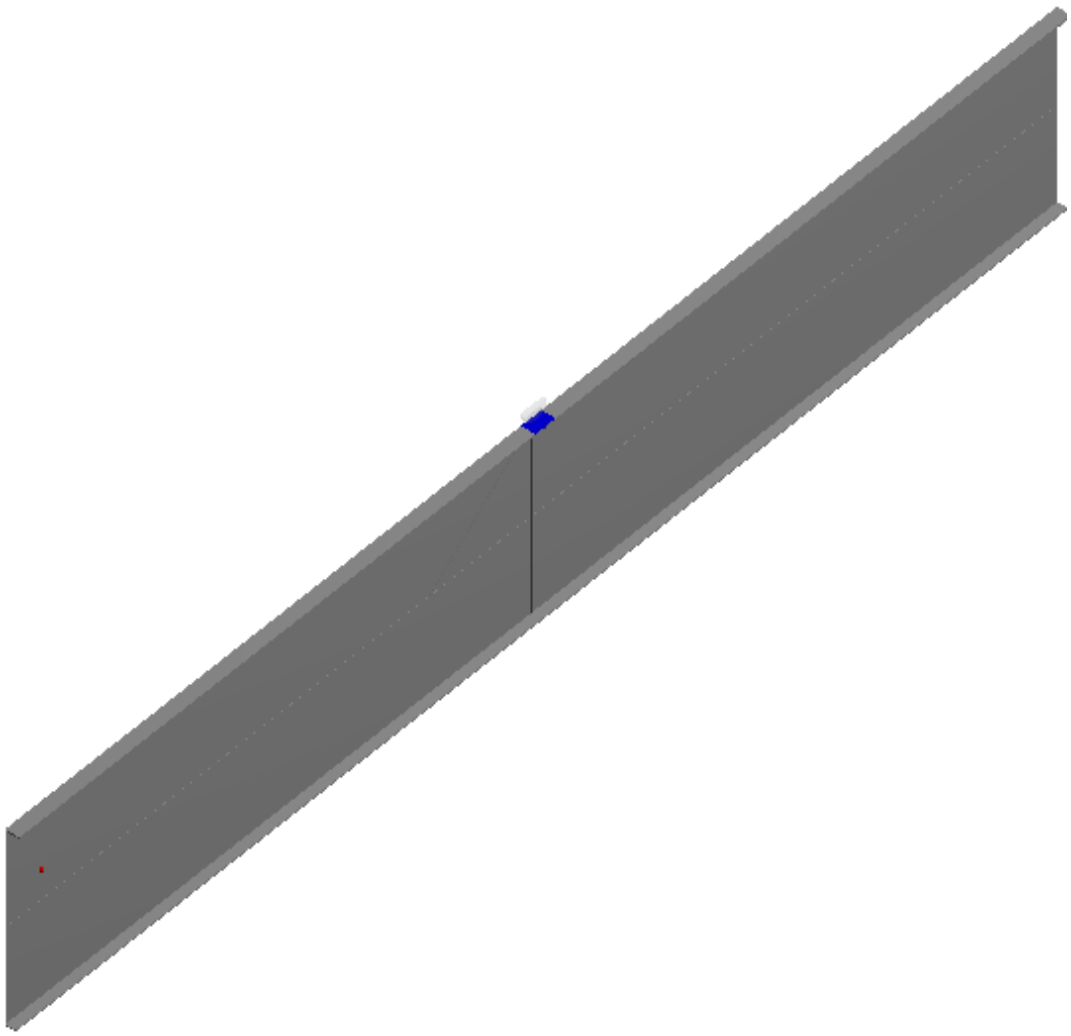

(b) Target surface

Figure 5.4 Contact modeling

5.3 Simplified modeling results

The simplified modeling is developed with a hexahedral mesh and compared with the field data again. The selected longitudinal strains of the lower surface of the bottom flange are compared at the launching stage between 823 ft to 824 ft.

The predicted strain for simplified modeling of the IRB Girder C at outer strain gages (COBF) and the center strain gage (CBF) on the lower surface of the steel girder bottom flange at stages 823.5 ft followed similar patterns to the field data and the original numerical modeling (see Figures 5.5).

The predicted strain from simplified modeling results at COBF differed from the original modeling about 7%, as shown in Figure 5.5 (a). As discussed in Chapter 4.3.2, the extreme strain from CBF were measured beyond stage 823.5 ft due to the gage were destroyed when they encountered the roller, thus the strains measured in the field around the stage 823.5 ft may not be reliable. The values could be a combination of the flange strain and gage strain itself due to the excessive pressure by the support roller. The maximum predicted longitudinal strains for simplified modeling validation under the bottom flange plate is approximately 2725 micro-strains (compression) and occur at the centerline of the lower surface of the bottom flange, as shown in Figure 5.5 (b). This is very similar to the original modeling (2870 micro-strains) discussed in Chapter 4.3.2. The difference between the simplified contact modeling and the original modeling is about 5%.

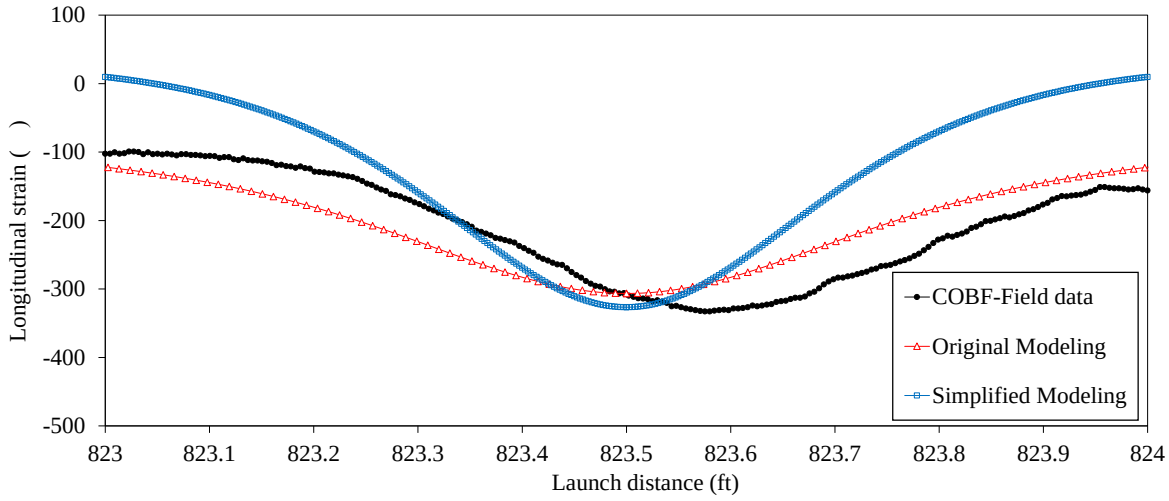

(a) Outer strain gages

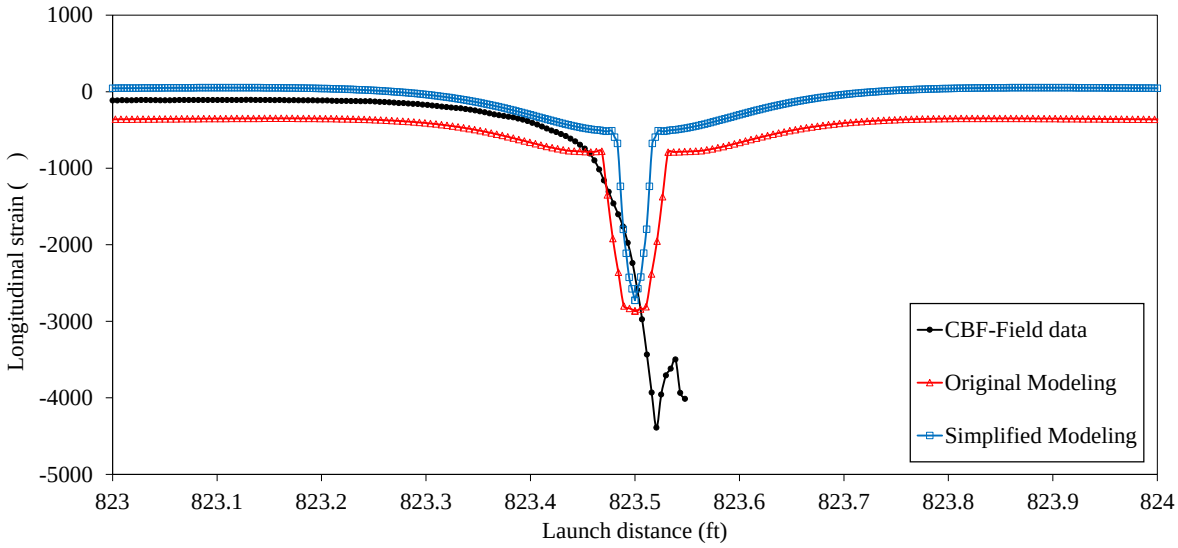

(b) Center strain gage

Figure 5.5 Longitudinal strain in the lower surface of the bottom flange

CHAPTER 6. CONTACT STRESS NOMOGRAM

Because a numerical modeling is not always applicable and convenient, this study proposes an approximate solution to estimate the contact stress between a bridge I-girder and a support roller using a nomogram. In order to create the nomogram, a parametric study needs several modeling with different variable. The variables considered in the parametric study are various roller dimension and vertical load (reaction).

6.1 Modeling and analysis settings

For the numerical modeling setting, the contact stress validation results from the simplified contact modeling illustrated in Chapter 5 were used to modify the roller diameters (d), a roller widths (l), and loads (F) (see Figure 6.1). Hexahedral mesh is used in each geometry and a single load is applied at the roller while the top surface of the top flange is fixed. Similar to the previous modeling, half of the lower surface of the bottom flange can be defined as a target element surface, and half of the roller surface is designed as a contact element surface with the contact friction coefficient of 0.3.

In the parametric modeling, the load from 5 kips to 25 kips was applied to the top surface of the roller support, the variable of roller diameter was set from 14 inches to 22 inches, and the roller width was changed from 5 inches to 8 inches. Selected parametric modeling input are listed in Tables 6.1, 6.2 while Appendix A shows all other cases.

6.2 Parametric modeling results

In order to develop a nomogram, about 180 simplified numerical models as a parametric study were generated with different variables. The variables considered in creating the nomogram are vertical reaction, the roller diameter, and contact length (the roller with). This was determined based on the variable discussed in Hertz contact theory. Tables 6.1 and

6.2 shows part of data that were used in development of the proposed contact stress nomogram. All results from other cases are available in Appendix A.

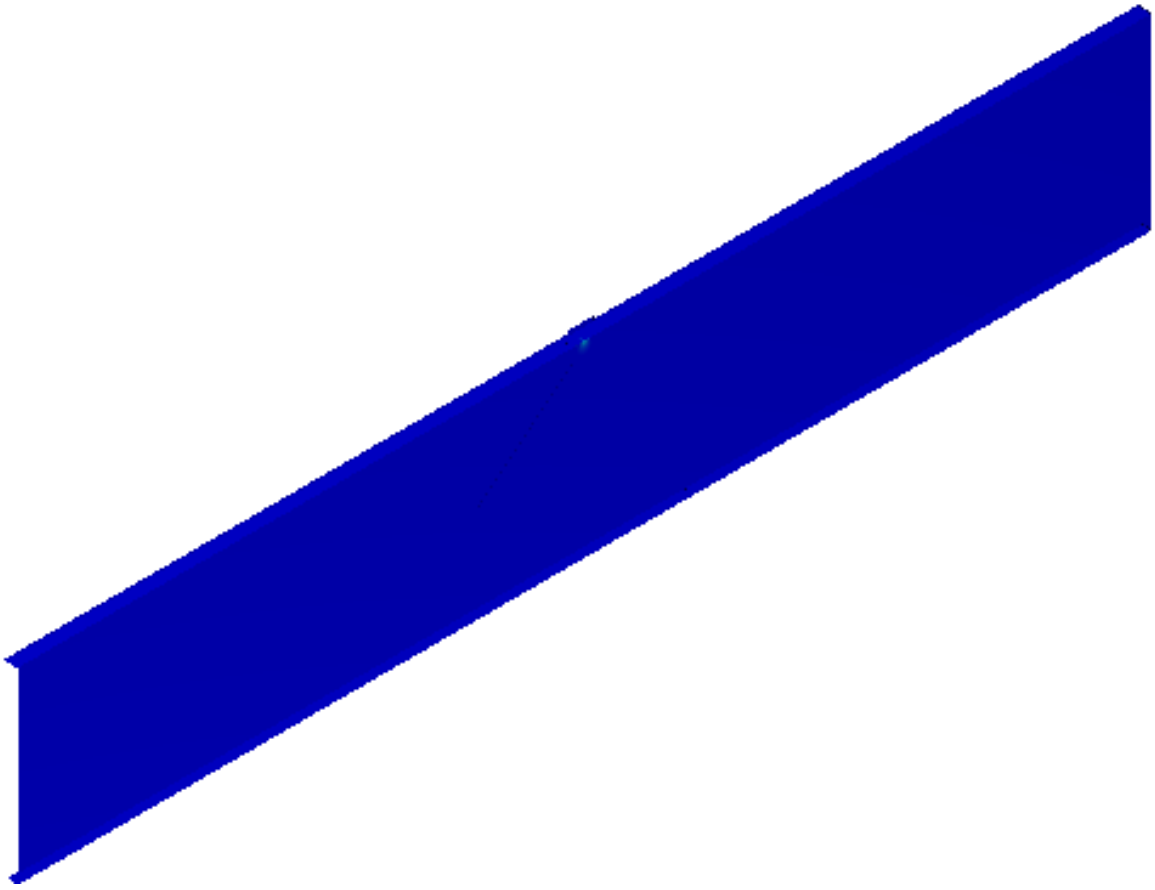

(a) Isometric view

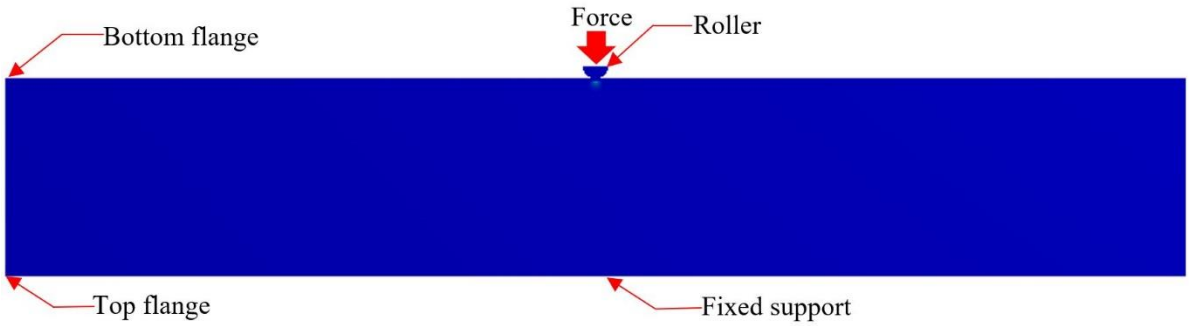

(b) Front view

Figure 6.1 Geometry of the parametric modeling

Table 6.1 Numerical modeling with a constant roller width of 6 inches

Variable Parameter			**Numerical Modeling Results**
Roller width (in.)	**Force (kips)**	**Roller diameter (in.)**	**Maximum contact stress (ksi)**
6	5	14	18.06
6	5	16	17.58
6	5	18	16.57
6	5	20	16.08
6	5	22	15.80
6	10	14	36.11
6	10	16	35.17
6	10	18	33.14
6	10	20	32.16
6	10	22	31.60
6	15	14	54.17
6	15	16	52.75
6	15	18	49.71
6	15	20	48.23
6	15	22	47.40
6	20	14	72.23
6	20	16	70.34
6	20	18	66.28
6	20	20	64.31
6	20	22	63.19
6	25	14	90.28
6	25	16	87.93
6	25	18	82.86
6	25	20	80.38
6	25	22	78.99

Table 6.2 Numerical modeling with a constant roller diameter of 18 inches

Variable Parameter			**Numerical Modeling Results**
Roller width (in.)	**Force (kips)**	**Roller diameter (in.)**	**Maximum contact stress (ksi)**
5	5	18	21.50
6	5	18	16.57
7	5	18	15.67
8	5	18	11.23
5	10	18	43.00
6	10	18	33.14
7	10	18	31.33
8	10	18	22.45
5	15	18	64.50
6	15	18	49.71
7	15	18	43.22
8	15	18	33.68
5	20	18	86.01
6	20	18	66.28
7	20	18	57.62
8	20	18	44.90
5	25	18	107.51
6	25	18	82.86
7	25	18	70.08
8	25	18	56.12

6.3 Contact stress nomogram

The nomogram is developed by numerical modeling to estimate the maximum contact stress between the launched roller and the bottom surface of the steel I-girder. The proposed nomogram consists of four parallel scales as shown in Figure 6.2. The leftmost and right-side scales are designated the input variables, consisting of the roller profile and total load identifying their values. The middle scale on the left side of the turning axis (T) represents the designated maximum contact stress for the input variables in the simplified modeling.

For the nomogram creating, the maximum contact stress was collected from the variables of force changed from 5 kips to 25 kips, the roller diameter increases from 14 inches to 22 inches, and the contact length (roller width) varies from 5 inches to 8 inches. The resulting plots in the nomogram indicate that the numerical modeling results of the contact stress correspond with the small contact point.

The advantage of the proposed nomogram is easy and quick estimation of maximum contact stress in the bridge girder. However, the numerical modeling used for the nomogram was based on the linear analysis and if the maximum contact stress is above the yield strength of the material, the nomogram is not applicable to define the accurate contact stress. A further numerical modeling is required for the case.

To determine the approximate maximum contact stress using the proposed nomogram, the following steps are required. First, locate measuring length of contact (roller width) and force on the appropriate scales and connect these points until the turning axis (T) is intersected. Next, locate the roller diameter and connect with the intersected T axis. Finally, read the maximum contact stress to be expected with thin the contact area.

For example, for a force of 15 kips, a contact length (roller width) of 6 inches, and a roller diameter of 18 inches, the maximum contact stress meets a value of 50 ksi (see blue dash line in Figure 6.2). As another example, a force of 5 kips, a contact length (roller width) of 5 inches, and a roller diameter of 22 inches are provided, then the maximum contact stress between roller and bottom surface of the steel I-girder is determined to be approximately 18 ksi (see solid black line in Figure 6.2). If a force of 25 kips, a contact length (roller width) of 8 inches, and a roller diameter of 14 inches are provided, then the maximum contact stress is approximately 70 ksi (see solid red line in Figure 6.2).

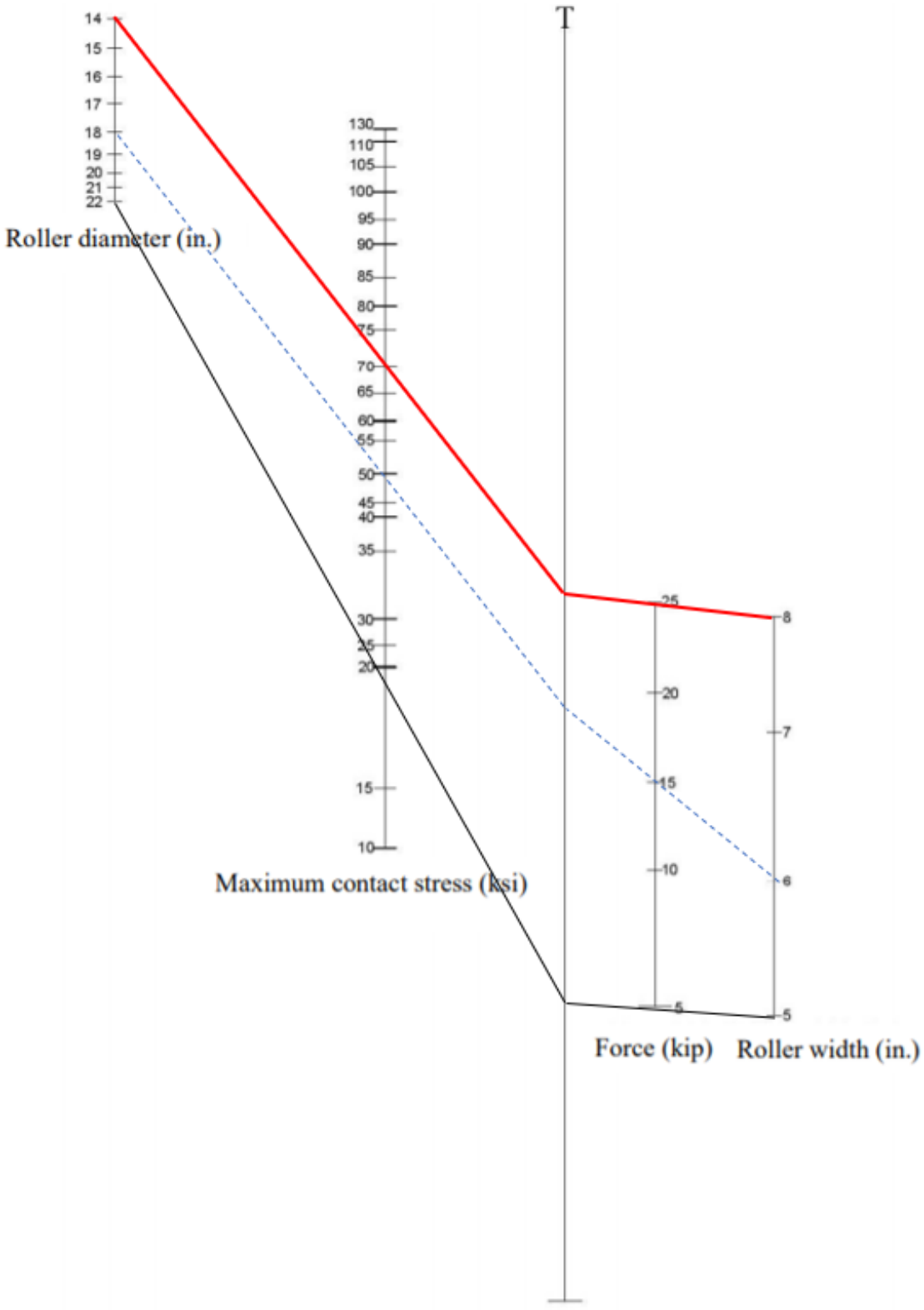

Figure 6.2 Maximum contact stresses nomogram

CHAPTER 7. SUMMARY AND CONCLUSIONS

7.1 Summary

The purpose of this study is to estimate the relationship of the maximum contact stress between an I-girder and a roller using a nomogram. The proposed nomogram is built based on a parametric study with various roller dimensions and loads by numerical modeling. This study began with a preliminary modeling of the cylindrical contact to validate the Hertz contact theory and followed by validation modeling with Iowa River Bridge. A parametric study with a simplified numerical modeling was performed with various roller dimension and vertical load to develop a nomogram.

7.2 Conclusions

The majority of the following conclusions have been verified using numerical modeling. Mesh style and size near the contact region is significant in improving the result accuracy. The important factors that influence the contact stress between an I-girder and a roller are vertical force near the contact area, roller diameter, and contact length (roller width). The vertical force impacts the contact stress significantly. While the bending moment has minimal influence around the contact region, the only shear at the end of the member and self-weight of the geometry is considered a single load. The nomogram is applicable to estimate the approximate contact stress between the bottom flange and roller in the elastic stage. If the contact stress is above the yield strength, further numerical modeling is required.

REFERENCES

Adams, G., & Nosonovsky, M.)2000(. Contact modeling-forces. *Tribology International*, 33, 431-442.

Antoine, J. F., Abba, G., C., V., & Sauvey, C.)2006(. Approximate analytical model for Hertzian elliptical contact problems. *Tribology International*, 1-10.

Budynas, R. G., & Nisbett, K. J.)2015(. *Mechanical engineering design.* New York: McGraw-Hill Education.

Chacon, R., Uribe, N., & Oller, S.)2013(. Numerical validation of the incremental launching method of a steel bridge through a small scale experimental study. *Society for Experimental Mechanics*, 40, 333-346.

Chang, B. I.)2004(. *Recommendations for the analysis of contact stresses for launched plate girder.* Ames, Iowa: Iowa State University.

Cifuentes, A. O., & Kalbag, A.)1992(. A performance study of tetrahedral and hexahedral elements in 3-D finite element structural analysis. *Elsevier Science*, 313-318.

Fischer, F. D., & Wiest, M.)2008(. Approximate analytical model for Hertzian elliptical wheel rail or wheel crossing contact problems. *Tribology International*, 130, 044501-1.

Granath, P.)1997(. Behavior of slender plate girders subjected to patch loading. *Constructional Steel Research*, 42, 1-19.

Granath, P.)1998(. Distribution of support reaction against a steel girder on a launching shoe. *Constructional Steel Research*, 47, 245 270.

Gupta, B., Choubey, A., & Varde, G. V.)2012(. Contact stress analysis of spur gear. *International Journal of Engineering Research & Technology (IJERT)*, 1, 1-7.

Hertz, H.)1896(. The principles of mechanics. *Miscellaneous Papers*. London: Macmillan & Co.

Holmes, M., & Mason, P.)1972(. Stresses in deep beams. *Building Science*, 7, 225-232.

LaViolette , M.)2007(. *Bridge construction practices using incremental launching.* Ames, Iowa: Center for Transportation Research and Education Iowa State University.

Lee, H. H.)2017(. *Finite element simulations with ANSYS Workbench 17.* Taiwan: SDC publications.

Mijovi, B., & Oklo, M. D.)2000(. Numerical model of a Hertz contact between two elastic solids. *Engineer Modelling*, 111-117.

Norden, B. N.)1973(. *On the compression of a cylinder in contact with a plane surface.* Washington, D. C.: Institute for Basic Standards.

Shepherd, J., & Johnson, C.)2006(. Hexahedral mesh generation constraints. *Springer Nature*, 195 213.

Shiao, M. C., & Chamis, C. C.)1992(. Mapping Methods for computationally efficient and accurate structural reliability. *33rd Structures, Structural Dynamics and Materials Conference.* Dallas,Texas: NASA Technical Memorandum.

Sladkowski, A., & Sitarz, M.)2003(. Analysis of wheel rail interaction using FE software. In J. R. A. Ekberg, *Wear*)pp. 1217-1223(. Katowice 40-019, Poland: ELSEVIER.

Srivastava, J., Sarkar, P., & Ranjan, V.)2014(. Contact stress analysis in wheel rail by Hertzian method and finite element method. *Springer Nature*, 95, 319 325.

Tanaka, N.)2001(. A new calculation method of Hertz elliptical contact pressure. *Tribology International*, 123)4(, 887-889.

Thorwald, G., & Vargas, P.)2017(. Cylinder axial crack reference stress comparison using elastic plastic FEA 3D crack mesh J-integral values. *Proceedings of the ASME 2017 Pressure Vessels and Piping Conference*)pp. 1-9(. Waikoloa, Hawaii, United States: ASME.

Wipf, T. J., Phares, B. M., Abendroth, R. A., Wood, D. L., Chang, B. I., & Abraham , S.)2004(. *Monitoring of the launched girder bridge over the Iowa river on US 20.* Ames, IA: Center for Transportation Research and Education Iowa State University.

Wriggers, P.)1996(. Finite element methods for contact problems with friction. *Tribology International*, 29, 651-658.

Xie , M., & Adams , D.)1995(. Contact finite element modeling of the short beam shear test for composite materials. *Computers & Structures*, 57, 183-191.

Zhao, X., & Li, Z.)2014(. A three-dimensional finite element solution of frictional wheel rail rolling contact in elasto-plasticity. *Tribology International*, 229, 86 100.

APPENDIX A. NUMERICAL MODELING RESULTS

Table A.1 Numerical modeling with a constant roller width of 5 inches

Variable Parameter			**Numerical Modeling Results**
Roller width (in.)	**Force (kips)**	**Roller diameter (in.)**	**Maximum contact stress (ksi)**
5	5	14	29.56
5	5	16	27.52
5	5	18	21.50
5	5	20	20.57
5	5	22	17.96
5	10	14	59.13
5	10	16	44.08
5	10	18	43.00
5	10	20	41.14
5	10	22	35.91
5	15	14	67.21
5	15	16	66.12
5	15	18	64.50
5	15	20	58.32
5	15	22	53.87
5	20	14	91.57
5	20	16	90.15
5	20	18	86.01
5	20	20	77.77
5	20	22	71.82
5	25	14	114.99
5	25	16	109.19
5	25	18	107.51
5	25	20	97.21
5	25	22	89.78

Table A.2 Numerical modeling with a constant roller width of 7 inches

Variable Parameter			**Numerical Modeling Results**
Roller width (in.)	**Force (kips)**	**Roller diameter (in.)**	**Maximum contact stress (ksi)**
7	5	14	17.07
7	5	16	16.71
7	5	18	15.67
7	5	20	13.92
7	5	22	13.67
7	10	14	34.15
7	10	16	33.41
7	10	18	31.33
7	10	20	27.84
7	10	22	23.42
7	15	14	51.22
7	15	16	44.43
7	15	18	43.22
7	15	20	34.20
7	15	22	33.35
7	20	14	71.13
7	20	16	59.24
7	20	18	57.62
7	20	20	53.87
7	20	22	52.34
7	25	14	85.35
7	25	16	74.04
7	25	18	70.08
7	25	20	67.34
7	25	22	65.43

Table A.3 Numerical modeling with a constant roller width of 8 inches

Variable Parameter			**Numerical Modeling Results**
Roller width (in.)	**Force (kips)**	**Roller diameter (in.)**	**Maximum contact stress (ksi)**
8	5	14	13.96
8	5	16	12.67
8	5	18	11.23
8	5	20	10.95
8	5	22	8.00
8	10	14	27.92
8	10	16	23.54
8	10	18	22.45
8	10	20	21.90
8	10	22	18.00
8	15	14	41.89
8	15	16	34.85
8	15	18	33.68
8	15	20	32.86
8	15	22	29.00
8	20	14	55.85
8	20	16	50.68
8	20	18	44.90
8	20	20	43.81
8	20	22	39.00
8	25	14	76.22
8	25	16	63.35
8	25	18	56.12
8	25	20	54.76
8	25	22	53.00

Table A.4 Numerical modeling with a constant roller diameter of 14 inches

Variable Parameter			**Numerical Modeling Results**
Roller width (in.)	**Force (kips)**	**Roller diameter (in.)**	**Maximum contact stress (ksi)**
5	5	14	29.56
6	5	14	18.06
7	5	14	17.07
8	5	14	13.96
5	10	14	59.13
6	10	14	36.11
7	10	14	34.15
8	10	14	27.92
5	15	14	67.21
6	15	14	54.17
7	15	14	51.22
8	15	14	41.89
5	20	14	91.57
6	20	14	72.23
7	20	14	71.13
8	20	14	55.85
5	25	14	114.99
6	25	14	90.28
7	25	14	85.35
8	25	14	76.22

Table A.5 Numerical modeling with a constant roller diameter of 16 inches

Variable Parameter			**Numerical Modeling Results**
Roller width (in.)	**Force (kips)**	**Roller diameter (in.)**	**Maximum contact stress (ksi)**
5	5	16	27.52
6	5	16	17.58
7	5	16	16.71
8	5	16	12.67
5	10	16	44.08
6	10	16	35.17
7	10	16	33.41
8	10	16	23.54
5	15	16	66.12
6	15	16	52.75
7	15	16	44.43
8	15	16	34.85
5	20	16	90.15
6	20	16	70.34
7	20	16	59.24
8	20	16	50.68
5	25	16	109.19
6	25	16	87.93
7	25	16	74.04
8	25	16	63.35

Table A.6 Numerical modeling with a constant roller diameter of 20 inches

Variable Parameter			**Numerical Modeling Results**
Roller width (in.)	**Force (kips)**	**Roller diameter (in.)**	**Maximum contact stress (ksi)**
5	5	20	20.57
6	5	20	16.08
7	5	20	13.92
8	5	20	10.95
5	10	20	41.14
6	10	20	32.16
7	10	20	27.84
8	10	20	21.90
5	15	20	58.32
6	15	20	48.23
7	15	20	34.20
8	15	20	32.86
5	20	20	77.77
6	20	20	64.31
7	20	20	53.87
8	20	20	43.81
5	25	20	97.21
6	25	20	80.38
7	25	20	67.34
8	25	20	54.76

Table A.7 Numerical modeling with a constant roller diameter of 22 inches

Variable Parameter			**Numerical Modeling Results**
Roller width (in.)	**Force (kips)**	**Roller diameter (in.)**	**Maximum contact stress (ksi)**
5	5	22	17.96
6	5	22	15.80
7	5	22	13.67
8	5	22	8.00
5	10	22	35.91
6	10	22	31.60
7	10	22	23.42
8	10	22	18.00
5	15	22	53.87
6	15	22	47.40
7	15	22	33.35
8	15	22	29.00
5	20	22	71.82
6	20	22	63.19
7	20	22	52.34
8	20	22	39.00
5	25	22	89.78
6	25	22	78.99
7	25	22	65.43
8	25	22	53.00